LETTER

doi:10.1038/nature14216

MAD2L2 controls DNA repair at telomeres and DNA breaks by inhibiting 5′ end resection

Vera Boersma[1]*, Nathalie Moatti[1]*, Sandra Segura-Bayona[1], Marieke H. Peuscher[1], Jaco van der Torre[1], Brigitte A. Wevers[1], Alexandre Orthwein[2], Daniel Durocher[2,3] & Jacqueline J. L. Jacobs[1]

Appropriate repair of DNA lesions and the inhibition of DNA repair activities at telomeres are crucial to prevent genomic instability. By fuelling the generation of genetic alterations and by compromising cell viability, genomic instability is a driving force in cancer and ageing[1,2]. Here we identify MAD2L2 (also known as MAD2B or REV7) through functional genetic screening as a novel factor controlling DNA repair activities at mammalian telomeres. We show that MAD2L2 accumulates at uncapped telomeres and promotes non-homologous end-joining (NHEJ)-mediated fusion of deprotected chromosome ends and genomic instability. MAD2L2 depletion causes elongated 3′ telomeric overhangs, indicating that MAD2L2 inhibits 5′ end resection. End resection blocks NHEJ while committing to homology-directed repair, and is under the control of 53BP1, RIF1 and PTIP[3]. Consistent with MAD2L2 promoting NHEJ-mediated telomere fusion by inhibiting 5′ end resection, knockdown of the nucleases CTIP or EXO1 partially restores telomere-driven genomic instability in MAD2L2-depleted cells. Control of DNA repair by MAD2L2 is not limited to telomeres. MAD2L2 also accumulates and inhibits end resection at irradiation-induced DNA double-strand breaks and promotes end-joining of DNA double-strand breaks in several settings, including during immunoglobulin class switch recombination. These activities of MAD2L2 depend on ATM kinase activity, RNF8, RNF168, 53BP1 and RIF1, but not on PTIP, REV1 and REV3, the latter two acting with MAD2L2 in translesion synthesis[4]. Together, our data establish MAD2L2 as a crucial contributor to the control of DNA repair activity by 53BP1 that promotes NHEJ by inhibiting 5′ end resection downstream of RIF1.

As the processes underlying telomere-driven genomic instability are not completely understood, we performed a functional genetic screen to identify telomere-induced genomic instability regulators (TIGIRs). The TIGIR screen relies on well-controlled reversible inactivation of telomere component TRF2 by expressing temperature-sensitive TRF2(Ile468Ala) (TRF2ts) in $Trf2^{-/-}$ $p53^{-/-}$ (also known as $Terf2^{-/-}$ $Trp53^{-/-}$) mouse embryo fibroblasts (MEFs)[5]. At the permissive temperature (32 °C), the TRF2ts MEFs have intact TRF2-mediated telomere protection, but at non-permissive temperatures (37–39 °C) TRF2ts is inactive, causing ATM kinase activation, accumulation of DNA damage response (DDR) proteins and NHEJ-dependent ligation at chromosome ends[5]. In the TIGIR screen (Fig. 1a), prolonged TRF2-inactivation causes TRF2ts cells to irreversibly arrest or die owing to severe chromosome end fusion that drives cells into genomic crisis[6–8]. However, diminished telomere fusion, such as with RNF8 or DNA ligase IV deficiency, allows survival and proliferation despite telomere uncapping[9–11].

In a triplicate TIGIR screen we assayed 1,976 short hairpin RNAs (shRNAs), targeting 391 genes linked to DDR, for shRNAs that allow TRF2ts cells to survive 12 days of telomere uncapping. Among shRNA targets substantially enriched in at least two out of three screens were several factors previously shown to control telomere fusion (Extended Data Fig. 1a, b), including ATM, NBS1, RAD50, 53BP1 and RNF8 (refs 11–15). Remarkably, the most prominent screen hit, also independently recovered in a genome-wide TIGIR screen (our unpublished results), was MAD2L2 (Extended Data Fig. 1a, b). MAD2L2 has no known function at telomeres but acts as a non-catalytic interaction partner of REV1 and REV3 in translesion synthesis[4]. Knockdown of *Mad2l2* with independent shRNAs markedly increased the survival of TRF2ts MEFs subjected to telomere uncapping, which was abolished by complementation with exogenous shRNA-resistant human *MAD2L2* (Fig. 1b, c and Extended Data Fig. 1c–f). Interestingly, we failed to detect a similar activity for REV1 or REV3 (Extended Data Fig. 1g–i).

Indeed, enhanced survival of MAD2L2-depleted cells after long-term TRF2 inactivation was due to diminished telomere fusion. *Mad2l2* knockdown significantly reduced telomere fusions, which was prevented by complementation with exogenous *MAD2L2* (Fig. 2a and Extended Data Fig. 2a). Telomeres end with a single-stranded 3′ G-overhang that undergoes DNA-ligase-IV/NHEJ-dependent degradation after loss of TRF2-mediated telomere protection[9,10]. Analysis of telomeric 3′ G-overhangs showed that MAD2L2 depletion prevents overhang loss at 48 h of TRF2 inactivation, further confirming that MAD2L2 is essential for efficient processing of deprotected telomeres by NHEJ (Fig. 2b and Extended Data Fig. 2b). The defect in NHEJ-mediated telomere fusion in *Mad2l2*-knockdown cells was not explained by changes in cell-cycle progression (Fig. 1b, 32 °C panels, and Extended Data Figs 1e and 2c, d). Moreover, MAD2L2 is essential for sister-telomere fusion after activation of DNA repair in mitosis[16] (Extended Data Fig. 2e). In line

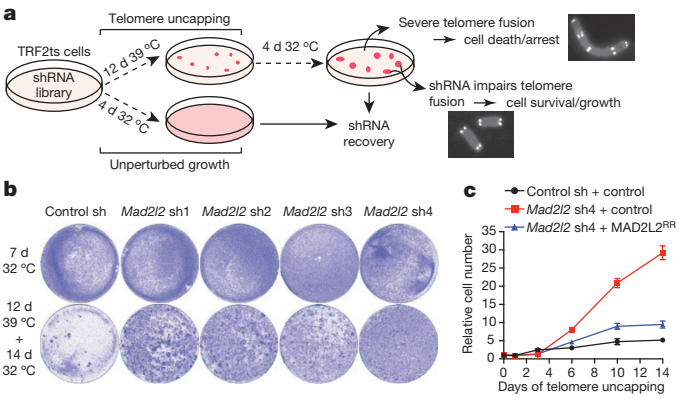

Figure 1 | A functional genetic screen identifies MAD2L2 as a critical factor in telomere-driven genomic instability. a, Outline of TIGIR screen to identify factors controlling telomere-driven genomic instability. d, day. **b**, Survival assays of TRF2ts MEFs infected with control shRNA (sh) or *Mad2l2* shRNAs (sh1–sh4), stained after growth as indicated. **c**, Growth curves at 39 °C of TRF2ts cells transduced with control or *Mad2l2* sh4 shRNAs and complemented with empty control or RNA interference (RNAi)-resistant Flag–MAD2L2^{RR} (data are mean ± s.d. from quadruplicate technical replicates).

[1]Division of Molecular Oncology, The Netherlands Cancer Institute, Plesmanlaan 121, 1066 CX, Amsterdam, The Netherlands. [2]The Lunenfeld-Tanenbaum Research Institute, Mount Sinai Hospital, 600 University Avenue, Toronto, Ontario M5G 1X5, Canada. [3]Department of Molecular Genetics, University of Toronto, Ontario M5S 3E1, Canada.
*These authors contributed equally to this work.

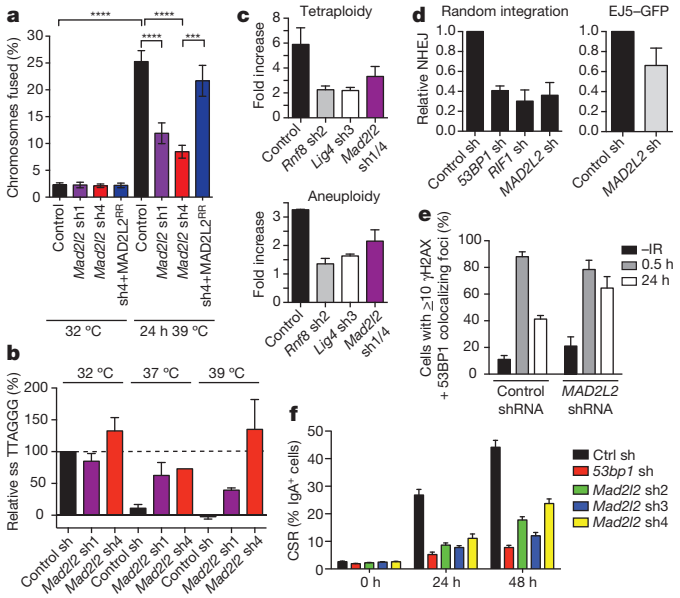

Figure 2 | MAD2L2 facilitates telomeric G-overhang degradation, NHEJ-mediated telomere fusion, repair and CSR. **a**, Chromosome fusion in shRNA-transduced TRF2ts MEFs ($n = 2$–4, mean ± s.e.m., $^{***}P = 0.0002$, $^{****}P < 0.0001$, Kruskal–Wallis analysis of variance (ANOVA)). **b**, Telomeric single-stranded (ss) G-overhang quantification in TRF2ts MEFs at 32 °C and after 48 h at 37 °C or 39 °C ($n = 4$, except *Mad2l2* sh4 at 37 °C: $n = 1$, mean ± s.e.m.). **c**, Tetraploidy (top) and aneuploidy (bottom) after telomere uncapping in TRF2ts MEFs ($n = 2$, mean ± s.d.). **d**, NHEJ-mediated repair in U2OS cells analysed by random plasmid integration (left, $n = 3$) or an EJ5–GFP reporter containing green fluorescent protein (GFP) (right, $n = 6$, mean ± s.d.). **e**, MAD2L2 depletion impairs resolution of DDR foci after irradiation (2 Gy) in HDR-deficient (RAD51-depleted) U2OS cells, indicating defective NHEJ ($n = 2$, mean ± s.e.m.). **f**, CSR in shRNA-transduced CH12F3-2 cells ($n = 3$, mean ± s.d.). Ctrl, control.

with MAD2L2 promoting telomere fusion, chromosomal rearrangement and mis-segregation[6–8], MAD2L2 depletion prevented tetraploidy and aneuploidy after telomere uncapping (Fig. 2c and Extended Data Fig. 2f).

To address whether the requirement of MAD2L2 for NHEJ extends beyond telomeres, we investigated whether MAD2L2 depletion affects end-joining in other settings. Knockdown of human *MAD2L2* considerably impaired NHEJ-mediated repair of I-Sce1-induced DNA double-strand breaks (DSBs), NHEJ-mediated random plasmid integration, resolution of irradiation-induced DSBs in homology-directed repair (HDR)-deficient cells and clonogenic survival after irradiation, similar to depletion of the NHEJ-promoting factors 53BP1 and RIF1 (Fig. 2d, e and Extended Data Fig. 3a–e). Moreover, class switch recombination (CSR), a physiological process depending on joining of DNA DSBs by NHEJ[17], was substantially impaired in MAD2L2-depleted cells (Fig. 2f and Extended Data Fig. 3f–i). This CSR defect was not due to defects in cell proliferation or expression of *Aid* (also known as *Aicda*) messenger RNA, IgM and IgA germ-line transcripts. Thus, MAD2L2 promotes NHEJ-mediated repair in several contexts.

To investigate how MAD2L2 promotes NHEJ, we first addressed its localization. MAD2L2 accumulated both at TRF2-deprotected telomeres and irradiation-induced DSBs (Fig. 3a), implying a direct activity of MAD2L2 at these sites. Next we examined activation of the DDR. At 3, 6 and 12 h of TRF2 inactivation, both control and MAD2L2-depleted cells activated ATM, phosphorylated H2AX, KAP1 and CHK2 (γH2AX, p-KAP1 and p-CHK2, respectively), and formed p-ATM and γH2AX foci to a similar extent (Fig. 3b, c and Extended Data Fig. 4a, b). Moreover, accumulation of 53BP1, RIF1 and PTIP to uncapped telomeres, as well as irradiation-induced DSBs, was unperturbed in MAD2L2-depleted cells (Fig. 3c and Extended Data Fig. 4a–c). Thus, MAD2L2 is not required for recognition of uncapped telomeres or DSBs as damage, nor for initiation of DDR signalling. However, probably reflecting aberrant processing of deprotected telomeres, we noticed increased DDR signalling at 24 and 48 h of TRF2 inactivation in MAD2L2-depleted cells,

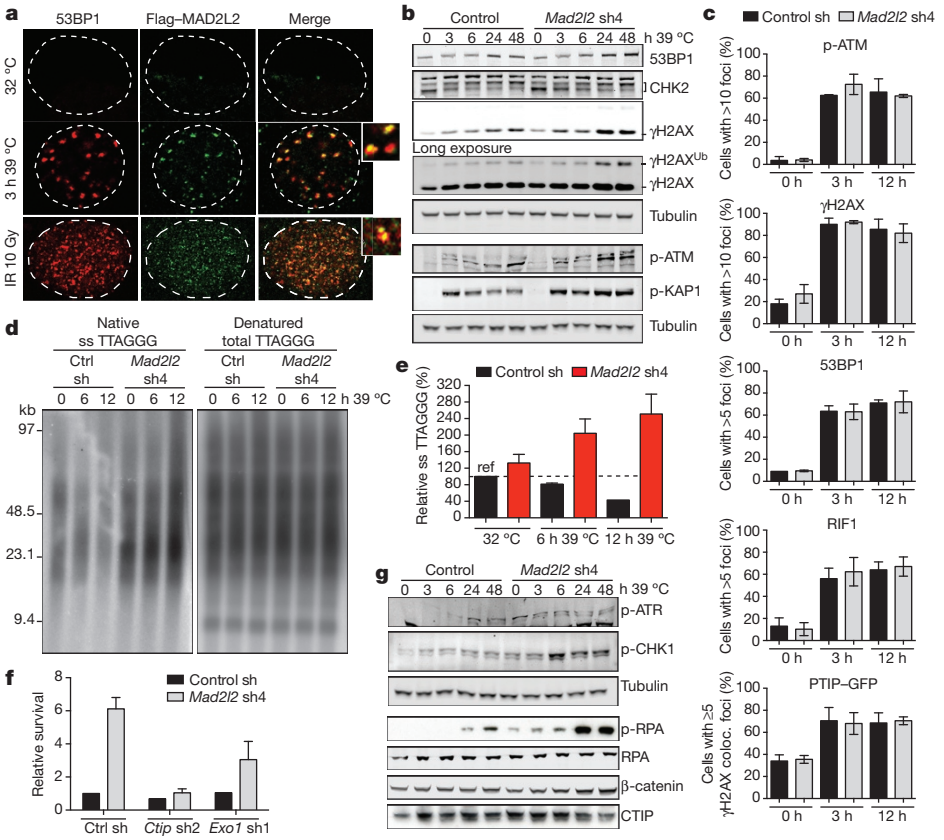

Figure 3 | MAD2L2 inhibits end resection and promotes telomere-induced genomic instability in a CTIP- and EXO1-dependent manner. **a**, Flag–MAD2L2 and 53BP1 localization in TRF2ts MEFs at 32 °C and 39 °C, and in $p53^{-/-}$ MEFs after ionizing radiation (IR). Original magnifications, ×63 with zoom factor 3. **b**, Immunoblotting for DDR factors in TRF2ts MEFs upon telomere uncapping at 39 °C. **c**, p-ATM, γH2AX, 53BP1, RIF1 and PTIP–GFP foci in TRF2ts MEFs grown for 0, 3 or 12 h at 39 °C ($n = 2$, mean ± s.d.). **d**, **e**, Representative example (**d**) and quantification (**e**) of telomeric single-stranded G-overhang analysis in TRF2ts MEFs grown as specified ($n = 3$, mean ± s.e.m.). **f**, Quantification of survival assays of TRF2ts MEFs shRNA-transduced as indicated ($n = 2$, mean ± s.e.m.). **g**, Immunoblotting for p-ATR(Ser 428), p-CHK1(Ser 345), p-RPA32(Ser 4/Ser 8), RPA34 and CTIP in TRF2ts MEFs upon telomere uncapping at 39 °C.

visible as increased H2AX and KAP1 phosphorylation, and H2AX ubiquitylation (Fig. 3b).

Next we examined the terminal structure of telomeres in more detail. Analysis of 3′ single-stranded G-overhangs at 6 and 12 h of TRF2 inactivation revealed that in the absence of MAD2L2, telomeres gain considerably longer 3′ single-stranded overhangs. At 12 h, *Mad2l2*-knockdown cells contained 2.5-fold higher, 3′-exonuclease sensitive overhang signals than control cells without uncapping, and nearly sixfold higher overhang signals than control cells at 12 h of telomere uncapping (Fig. 3d, e and Extended Data Fig. 5a). Overhang increase upon MAD2L2 depletion was observed in both wild-type and DNA-ligase-IV-deficient TRF2ts cells (Extended Data Fig. 5b–d), indicating it is not a passive consequence of lack of NHEJ-mediated overhang degradation, but represents an active role of MAD2L2 in inhibiting 5′ end resection. 5′ DNA end resection is a powerful obstruction to NHEJ by creating DNA ends unsuitable for ligation[18], explaining why MAD2L2 depletion impairs NHEJ-mediated repair.

5′ end resection involves the combined activities of CTIP, MRN, EXO1, BLM and DNA2, and is blocked by 53BP1 and its interaction partners RIF1 and PTIP[3,13,19–24]. In line with MAD2L2 promoting NHEJ by impeding 5′ end resection, co-depletion of CTIP or EXO1 with MAD2L2 partially reversed the increased survival of *Mad2l2*-knockdown cells undergoing prolonged telomere uncapping (Fig. 3f and Extended Data Fig. 5e–h). Moreover, consistent with the generation of longer single-stranded overhangs that block NHEJ and prime for HDR, *Mad2l2*-knockdown cells showed increased phosphorylation of the ATR target CHK1 and of the single-stranded DNA-binding protein RPA (Fig. 3g). In addition, MAD2L2-depleted cells showed increased HDR at telomeres by increased telomere sister-chromatid exchanges (TSCE; Extended Data Fig. 6a).

Because the effects of MAD2L2 depletion on end resection, telomere fusion and CSR resemble those of 53BP1, RIF1 and, to a certain extent, PTIP inactivation[3,13,19–24], we asked whether MAD2L2 is epistatic with 53BP1, RIF1 or PTIP. Similarly, we addressed the requirement of REV1 and REV3 for the ability of MAD2L2 to control end resection and telomere fusion. Unlike in wild-type or PTIP-deficient MEFs, MAD2L2 depletion did not reduce fusion of TRF2-deprotected telomeres in 53BP1- or RIF1-deficient MEFs (Fig. 4a and Extended Data Fig. 6b–e). However, MAD2L2(Leu186Ala) and MAD2L2(Cys70Arg), defective in REV1 or REV3 interaction, respectively[25,26], were still capable of promoting telomere fusion and telomere-driven genomic instability (Fig. 4b and Extended Data Fig. 7a, g, i). Moreover, MAD2L2 depletion resulted in increased RPA phosphorylation after irradiation in wild-type, *Ptip*$^{-/-}$, *Rev1*$^{-/-}$ or *Rev3*$^{-/-}$ MEFs, but not in *53bp1*$^{-/-}$ (also known as *Trp53bp1*$^{-/-}$) or *Rif1*$^{-/-}$ MEFs (Fig. 4c). This indicates that MAD2L2 controls end resection and fusion of deprotected telomeres in a 53BP1- and RIF1-dependent, but PTIP-, REV1- and REV3-independent manner. Unanticipated, MAD2L2-depleted *Rif1*$^{-/-}$ MEFs showed an increased background of chromosome end fusion caused by telomere association between sister chromatids (Fig. 4a and Extended Data Fig. 6d, e). The molecular nature of these sister telomere associations remains to be determined, but they occur irrespective of TRF2 inhibition and potentially reflect replication problems[27].

To address the dependencies for MAD2L2 function in DNA repair further, we investigated the requirements for MAD2L2 accumulation to DSBs and NHEJ activity at telomeres. Both DSB accumulation and the ability to promote telomere-driven genomic instability by MAD2L2 require an intact HORMA domain and carboxy terminus, while potential S/TQ (Ser or Thr residues that precede Gln) phosphorylation on Thr 103 appears dispensable (Fig. 4b and Extended Data Fig. 7). Interestingly, while MAD2L2 accumulation to irradiation-induced DDR foci (IRIFs) was independent of PTIP or interaction of MAD2L2 with REV1 or REV3, it clearly depended on ATM kinase activity, RNF8, RNF168, 53BP1 and RIF1 (Fig. 4d, e and Extended Data Figs 7c, e and 8). More specifically, MAD2L2 IRIF accumulation required the HEAT repeats of RIF1 and the same ATM/ATR phosphorylation sites in 53BP1

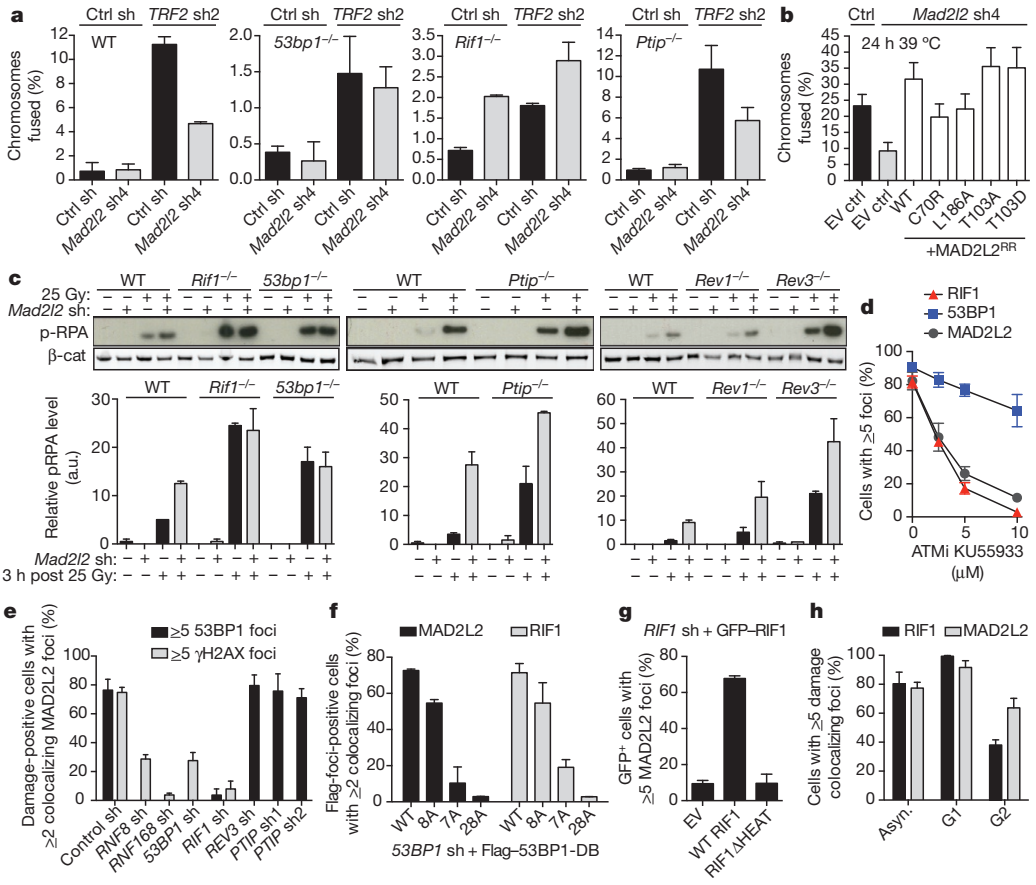

Figure 4 | MAD2L2 localizes to DSBs, inhibits end resection and promotes telomere-NHEJ in a 53BP1- and RIF1-dependent manner. **a**, Chromosome fusion after TRF2 inhibition in MEFs ($n = 2$, mean ± s.e.m.). WT (wild type) denotes controls to *53bp1*$^{-/-}$ and *Rif1*$^{-/-}$ MEFs. See Extended Data Fig. 6c for *Ptip*$^{+/+}$ MEFs. **b**, Chromosome fusion in TRF2ts MEFs (mean ± s.e.m.). EV, empty vector. **c**, p-RPA levels in MEFs ($n = 2$, mean ± s.e.m.). a.u., arbitrary units. **d**, Irradiation-induced MAD2L2, RIF1 and 53BP1 foci in ATM inhibitor (ATMi)-treated U2OS cells ($n = 3$, mean ± s.e.m.). **e**, MAD2L2 foci in irradiated shRNA-transduced U2OS cells ($n = 2$, mean ± s.d.). **f**, MAD2L2 and RIF1 foci in irradiated U2OS cells expressing 53BP1-DB alleles with wild-type or substituted S/TQ sites (schematic in Extended Data Fig. 9a; $n = 2$, mean ± s.d.). **g**, MAD2L2 foci in irradiated U2OS cells expressing wild-type RIF1 or RIF1 lacking heat repeats ($n = 2$, mean ± s.d.). **h**, MAD2L2 and RIF1 foci in irradiated asynchronous, G1 or G2 synchronized RPE cells ($n = 3$, mean ± s.d.).

that promote RIF1 IRIFs, while those that promote PTIP IRIFs were dispensable[21–24] (Fig. 4f, g and Extended Data Fig. 9a–c). Similarly, MAD2L2 localization to uncapped telomeres required 53BP1 (Extended Data Fig. 8e). In line with dependency on RIF1, whose localization to DSBs is strongly reduced in G2, MAD2L2 foci were also diminished in G2, although less than RIF1 foci (Fig. 4h and Extended Data Fig. 9d). The latter could relate to a proposed role for MAD2L2 in the late steps of HDR[28].

In addition to inhibiting end resection, 53BP1, but not RIF1, promotes NHEJ by increasing mobility of uncapped telomeres[13,20]. Consistent with MAD2L2 acting via end resection control downstream of RIF1, MAD2L2 deficiency did not impair mobility of uncapped telomeres (Extended Data Fig. 10a–c).

Altogether, our data identify MAD2L2 as an important regulator of DNA repair pathway choice that promotes NHEJ at telomeres and DSBs in multiple settings, by inhibiting CTIP- and EXO1-dependent 5′ end resection downstream of RIF1 (Extended Data Fig. 10d). Whether MAD2L2 affects regulatory acetylation or phosphorylation of CTIP[18], or blocks other end resection factors, awaits further investigation.

MAD2L2 and REV3 together compose Polζ and act with REV1 in translesion synthesis to facilitate DNA replication past blocking lesions[4]. On the basis of reduced gene conversion and impaired RPA foci, RAD51 foci and DSB resolution in REV1- and Polζ-depleted cells, it has been proposed that the ability of REV1/Polζ to alleviate replication stalling might also be important during HDR synthesis[28]. Although requiring further characterization, together with the data presented here, this suggests differential roles for MAD2L2 in DSB repair. As shown here, MAD2L2 acts downstream of 53BP1/RIF1 in a REV1/REV3-independent manner to promote NHEJ by inhibiting resection, mostly in G1. In addition, MAD2L2, as part of Polζ, might promote HDR by facilitating replication of damaged DNA formed after resection in G2.

The contribution of MAD2L2 to DNA repair at uncapped telomeres and DSBs suggests that aberrant MAD2L2 expression could have pathological consequences by compromising genome integrity. In this respect it is interesting that in particular MAD2L2, more than REV1 or REV3, is reported to be overexpressed in several cancers and has prognostic significance (ref. 29 and the Oncomine database). Furthermore, our finding that MAD2L2 is essential for CSR identifies MAD2L2 as a potential disease-susceptibility gene for human primary immunodeficiencies.

Online Content Methods, along with any additional Extended Data display items and Source Data, are available in the online version of the paper; references unique to these sections appear only in the online paper.

Received 17 February; accepted 29 December 2014.
Published online 23 March 2015.

1. Hanahan, D. & Weinberg, R. A. Hallmarks of cancer: the next generation. *Cell* **144,** 646–674 (2011).
2. López-Otin, C., Blasco, M. A., Partridge, L., Serrano, M. & Kroemer, G. The hallmarks of aging. *Cell* **153,** 1194–1217 (2013).
3. Zimmermann, M. & de Lange, T. 53BP1: pro choice in DNA repair. *Trends Cell Biol.* **24,** 108–117 (2014).
4. Waters, L. S. *et al.* Eukaryotic translesion polymerases and their roles and regulation in DNA damage tolerance. *Microbiol. Mol. Biol. Rev.* **73,** 134–154 (2009).
5. Konishi, A. & de Lange, T. Cell cycle control of telomere protection and NHEJ revealed by a ts mutation in the DNA-binding domain of TRF2. *Genes Dev.* **22,** 1221–1230 (2008).
6. O'Sullivan, R. J. & Karlseder, J. Telomeres: protecting chromosomes against genome instability. *Nature Rev. Mol. Cell Biol.* **11,** 171–181 (2010).
7. Davoli, T. & de Lange, T. The causes and consequences of polyploidy in normal development and cancer. *Annu. Rev. Cell Dev. Biol.* **27,** 585–610 (2011).
8. Murnane, J. P. Telomere dysfunction and chromosome instability. *Mutat. Res.* **730,** 28–36 (2012).
9. Smogorzewska, A., Karlseder, J., Holtgreve-Grez, H., Jauch, A. & de Lange, T. DNA ligase IV-dependent NHEJ of deprotected mammalian telomeres in G1 and G2. *Curr. Biol.* **12,** 1635 (2002).
10. Celli, G. B. & de Lange, T. DNA processing is not required for ATM-mediated telomere damage response after TRF2 deletion. *Nature Cell Biol.* **7,** 712–718 (2005).
11. Peuscher, M. H. & Jacobs, J. J. DNA-damage response and repair activities at uncapped telomeres depend on RNF8. *Nature Cell Biol.* **13,** 1139–1145 (2011).
12. Denchi, E. L. & de Lange, T. Protection of telomeres through independent control of ATM and ATR by TRF2 and POT1. *Nature* **448,** 1068–1071 (2007).
13. Dimitrova, N., Chen, Y. C., Spector, D. L. & de Lange, T. 53BP1 promotes non-homologous end joining of telomeres by increasing chromatin mobility. *Nature* **456,** 524–528 (2008).
14. Deng, Y., Guo, X., Ferguson, D. O. & Chang, S. Multiple roles for MRE11 at uncapped telomeres. *Nature* **460,** 914–918 (2009).
15. Dimitrova, N. & de Lange, T. Cell cycle-dependent role of MRN at dysfunctional telomeres: ATM signaling-dependent induction of nonhomologous end joining (NHEJ) in G1 and resection-mediated inhibition of NHEJ in G2. *Mol. Cell. Biol.* **29,** 5552–5563 (2009).
16. Orthwein, A. *et al.* Mitosis inhibits DNA double-strand break repair to guard against telomere fusions. *Science* **344,** 189–193 (2014).
17. Daniel, J. A. & Nussenzweig, A. The AID-induced DNA damage response in chromatin. *Mol. Cell* **50,** 309–321 (2013).
18. Panier, S. & Durocher, D. Push back to respond better: regulatory inhibition of the DNA double-strand break response. *Nature Rev. Mol. Cell Biol.* **14,** 661–672 (2013).
19. Sfeir, A. & de Lange, T. Removal of shelterin reveals the telomere end-protection problem. *Science* **336,** 593–597 (2012).
20. Zimmermann, M., Lottersberger, F., Buonomo, S. B., Sfeir, A. & de Lange, T. 53BP1 regulates DSB repair using Rif1 to control 5′ end resection. *Science* **339,** 700–704 (2013).
21. Di Virgilio, M. *et al.* Rif1 prevents resection of DNA breaks and promotes immunoglobulin class switching. *Science* **339,** 711–715 (2013).
22. Chapman, J. R. *et al.* RIF1 is essential for 53BP1-dependent nonhomologous end joining and suppression of DNA double-strand break resection. *Mol. Cell* **49,** 858–871 (2013).
23. Escribano-Díaz, C. *et al.* A cell cycle-dependent regulatory circuit composed of 53BP1–RIF1 and BRCA1-CtIP controls DNA repair pathway choice. *Mol. Cell* **49,** 872–883 (2013).
24. Callen, E. *et al.* 53BP1 mediates productive and mutagenic DNA repair through distinct phosphoprotein interactions. *Cell* **153,** 1266–1280 (2013).
25. Hara, K. *et al.* Crystal structure of human REV7 in complex with a human REV3 fragment and structural implication of the interaction between DNA polymerase zeta and REV1. *J. Biol. Chem.* **285,** 12299–12307 (2010).
26. Khalaj, M. *et al.* A missense mutation in Rev7 disrupts formation of Polzeta, impairing mouse development and repair of genotoxic agent-induced DNA lesions. *J. Biol. Chem.* **289,** 3811–3824 (2014).
27. Chan, K. L., Palmai-Pallag, T., Ying, S. & Hickson, I. D. Replication stress induces sister-chromatid bridging at fragile site loci in mitosis. *Nature Cell Biol.* **11,** 753–760 (2009).
28. Sharma, S. *et al.* REV1 and polymerase zeta facilitate homologous recombination repair. *Nucleic Acids Res.* **40,** 682–691 (2012).
29. Rimkus, C. *et al.* Expression of the mitotic checkpoint gene MAD2L2 has prognostic significance in colon cancer. *Int. J. Cancer* **120,** 207–211 (2007).

Acknowledgements We thank A. Konishi, G. Celli and T. de Lange for TRF2(Ile468Ala), $Trf2^{flox/-}$ $p53^{-/-}$ MEFs and $Trf2^{flox/-}$ $p53^{-/-}$ $Lig4^{-/-}$ MEFs, P. Bouwman, M. Pieterse, T. Halazonetis, O. Kallioniemi, B. Gerritsen, B. Morris and P. Halonen for composing and providing the DDR TRC shRNA sub-library, members of the NKI Genomics Core Facility for technical support, A. van Kessel for *MAD2L2* cDNA, E. Hendrickson for repair plasmids, R. Chapman and S. Boulton for mRIF1 antibody, $53bp1^{-/-}$ and $Rif1^{-/-}$ MEFs, E. Callen and A. Nussenzweig for 53BP1 and PTIP expression vectors and for $Ptip^{-/-}$ MEFs, N. de Wind for $Rev1^{-/-}$ and $Rev3^{-/-}$ MEFs, B. van den Broek for help with telomere mobility analysis, I. de Krijger, Z. Yalcin and M. Simonetta from the Jacobs group for contributing to end resection and interaction analysis and members of the R. Medema laboratory for discussion. This work was supported by grants from the European Research Council (ERCStG 311565) and Dutch Cancer Society (KWF-NKI2007-3907) to J.J.L.J., a grant from the Canadian Institutes for Health Research (CIHR MOP89754) to D.D., a La Caixa fellowship to S.S.B. and a CIHR post-doctoral fellowship to A.O. D.D. is a Canada Research Chair (tier 1) in the Molecular Mechanisms of Genome Integrity and J.J.L.J. is an EMBO Young Investigator.

Author Contributions J.J.L.J., V.B., N.M. and S.S.-B. designed the experiments and analysed the data. M.H.P. and J.v.d.T. performed the TIGIR-screen, analysed the screen results and performed initial validation. V.B., N.M., S.S.-B. and B.A.W. performed all experiments, with the exception of assessment of CSR and sister-telomere fusion upon repair activation in mitosis, which were performed and analysed by A.O. and D.D. S.S.-B., M.H.P. and J.v.d.T. contributed equally. J.J.L.J. wrote the manuscript.

Author Information Reprints and permissions information is available at www.nature.com/reprints. The authors declare no competing financial interests. Readers are welcome to comment on the online version of the paper. Correspondence and requests for materials should be addressed to J.J.L.J. (j.jacobs@nki.nl).

METHODS

TIGIR screen. *Trf2*$^{-/-}$ *p53*$^{-/-}$ TRF2ts MEFs (in short TRF2ts MEFs) were infected in triplicate with PLKO lentiviral shRNA pools consisting of 1,976 shRNAs selected from the Mouse TRC 1.0 Collection. Cells were infected with a multiplicity of infection below 1 and drug selected on 4 μg ml^{-1} puromycin. After completion of selection, TRF2ts MEFs were plated in duplicate on 15-cm dishes at 150,000 cells per dish and allowed to adhere at 32 °C. One set of plates was kept at 32 °C for 4 additional days, the other set of plates was subjected to 12 days of telomere uncapping at 39 °C, followed by recovery for 4 additional days at 32 °C. Cells were collected for genomic DNA isolation using a DNeasy Blood & Tissue Kit (Qiagen) and shRNA inserts were recovered from genomic DNA by 2 sequential PCR amplifications (PCR1 and PCR2). In PCR1 6 individual PCR reactions were performed on 325 ng genomic DNA using for each sample a common reverse primer P7_PLKO1_R (5′-CAAGCAGAAGACGGCATACGAGATTTCTTTCCCCTGCACTGTACCC-3′) and 1 of 6 forward primers with a unique index (underlined): Illuseq_01_PLKO1_f (5′-ACACTCTTTCCCTACACGACGCTCTTCCGATCTCGTGATCTTGTGGAAAGGACGAAACACCGG-3′), Illuseq_02_PLKO1_f (5′-ACACTCTTTCCCTACACGACGCTCTTCCGATCTACATCGCTTGTGGAAAGGACGAAACACCGG-3′), Illuseq_03_PLKO1_f (5′-ACACTCTTTCCCTACACGACGCTCTTCCGATCTGCCTAACTTGTGGAAAGGACGAAACACCGG-3′), Illuseq_04_PLKO1_f (5′-ACACTCTTTCCCTACACGACGCTCTTCCGATCTTGGTCACTTGTGGAAAGGACGAAACACCGG-3′), Illuseq_05_PLKO1_f (5′-ACACTCTTTCCCTACACGACGCTCTTCCGATCTCACTGTCTTGTGGAAAGGACGAAACACCGG-3′), Illuseq_06_PLKO1_f (5′-ACACTCTTTCCCTACACGACGCTCTTCCGATCTATTGGCCTTGTGGAAAGGACGAAACACCGG-3′). In PCR2, 2.5 μl DNA from each PCR1 reaction was amplified using primers P5_Illuseq (5′-AATGATACGGCGACCACCGAGATCTACACTCTTTCCCTACACGACGCTCTTCCGATCT-3′) and P7 (5′-CAAGCAGAAGACGGCATACGAGAT-3′). PCR products were pooled per condition, purified using a Qiagen PCR purification kit (Qiagen), analysed on a bioanalyzer for quality and concentration, and subjected to deep-sequencing on a Illumina Hiseq2000 genome analyser at the NKI Genomics Core Facility.

Cell culture, growth assays, flow-cytometry. *Trf2*$^{-/-}$ *p53*$^{-/-}$ TRF2ts MEFs (TRF2ts MEFs) and *Trf2*$^{-/-}$ *p53*$^{-/-}$ *Lig4*$^{-/-}$ TRF2ts MEFs (TRF2ts *Lig4*$^{-/-}$ MEFs) were generated from *Trf2*$^{flox/-}$ *p53*$^{-/-}$ MEFs and *Trf2*$^{flox/-}$ *p53*$^{-/-}$ *Lig4*$^{-/-}$ MEFs as described before[11]. All cells were grown in DMEM with 100 U penicillin, 0.1 mg ml^{-1} streptomycin, 2 mM L-glutamine and 10% FBS. TRF2ts MEFs were maintained at the permissive temperature of 32 °C and only grown at 37 °C or 39 °C to induce telomere uncapping through inactivation of TRF2. All other cells were grown at 37 °C. Wild-type, *53bp1*$^{-/-}$, *Rif1*$^{-/-}$, *Ptip*$^{+/+}$ and *Ptip*$^{-/-}$ MEFs were SV40 immortalized.

For colony survival assays, TRF2ts MEFs were plated at 150,000 cells per 15-cm dish or 45,000 per 10-cm dish, allowed to adhere and kept at 32 °C or placed at 39 °C. To evaluate potential toxicity or growth rate differences, plates were fixed with 10% formalin and stained with 0.1% crystal violet after growth for 1 week at 32 °C. To evaluate survival upon prolonged telomere uncapping plates were fixed and stained after growth for 12 days at 39 °C, followed by 0 or 2 weeks recovery at 32 °C. Quantifications of survival assays reflect the relative survival after growth for 12 days at 39 °C and 2 weeks recovery at 32 °C, corrected for plating efficiency and growth at 32 °C and assessed by crystal violet extraction as described below.

To address cell survival under telomere uncapping conditions in short-term growth assays, TRF2ts MEFs were plated in quadruplicate at 5,000 cells per well on a 12-well plate (Fig. 1c) or in duplicate at 2,500 cells per well on a 24-wells plate (Extended Data Fig. 5h), allowed to adhere overnight at 32 °C and then placed for 12–14 days at 39 °C. During this time period of non-permissive temperature, plates were fixed every 2–4 days with 10% formalin and stained with 0.1% crystal violet. Crystal violet was extracted from the plates using 10% acetic acid and its absorbance at 595 nm was quantified using a Tecan microplate reader. Quantifications were corrected for plating efficiency.

Cell cycle distribution of TRF2ts MEFs with or without MAD2L2 knockdown was determined by propidium iodide staining, as well as by BrdU incorporation, and acquired on a BD Fortessa using FACSDiva software (BD Biosciences) and analysed with FlowJo (TreeStar) software.

Analysis of tetraploidy (8*N*) and aneuploidy (>4*N*) was based on DNA-content analysis by flow cytometry of TRF2ts cells grown at 32 °C or 39 °C for 48 h and then stained with propidium iodide.

Cell cycle synchronisation was done as follows. For G1 cells, RPE cells were kept in 2.5 mM thymidine (T1895, Sigma) for 16 h, released for 6 h, treated with 10 μM RO3306 (Calbiochem) for 16 h. Synchronised cells were released for 1 h, mitotic cells were collected by mitotic shake off and replated to let them continue into G1 3.5 h before irradiation.

For G2 cells, RPE cells were kept in 2.5 mM thymidine for 16 h, released for 6 h and treated with 2.5 mM thymidine for 16 h. Synchronised cells were released for 4.5 h before irradiation to let cells progress to G2.

Plasmids. Cells were transduced as before[11] with the following pLKO-puro shRNA lentiviruses obtained from Mission library clones (Sigma) against mouse genes: *Mad2l2* sh1 (TRCN0000012843: 5′-CCAGACTCCAAGTGCTCTTAT-3′), *Mad2l2* sh2 (TRCN0000012844: 5′-CCAGTGGAGAAGTTTGTCTTT-3′), *Mad2l2* sh3 (TRCN0000012845: 5′-CGAGCCTTCATCCTTAAGATT-3′), *Mad2l2* sh4 (TRCN0000012846: 5′-CATCTTCCAGAAGCGCAAGAA-3′), *Rev1* sh pool (pool of TRCN0000120297: 5′-CAGCAGTGCTTGTGAGGTATT-3′, TRCN0000120298: 5′-GCCGAGATCAACTATGGAATA-3′, TRCN0000120299: 5′-GCTGGAATGAAGACGGTGTAA-3′, TRCN0000120300: 5′-GCCCTCCGTATTGAAATCAAA-3′, TRCN0000120301: 5′-GCACGTTGATATGGACTGCTT-3′), *Rev1* sh1 (TRCN0000120298: 5′- GCCGAGATCAACTATGGAATA-3′), *53bp1* sh1 (TRCN0000081778: 5′-GCTATTGTGGAGATTGTGTTT-3′ and against human genes: *MAD2L2* sh (TRCN0000006570: 5′-CCCGGAGCTGAATCAGTATAT-3′), *53BP1* sh (TRCN0000018865: 5′-GATACTTGGTCTTACTGGTTT-3′), *RIF1* sh (TRCN0000155431: 5′-CGCATTCTGCTGTTGTTGATT-3′), *PTIP* sh1 (TRCN0000129174: 5′-CTTCAGATTCATCACCGGAAA-3′), *PTIP* sh2 (TRCN0000322819: 5′-GCCATGTTCACAGCATATTAT-3′), *RNF8* sh: (TRCN0000003439: 5′-GAAGCCGTTATGAATGTGAAA-3′), *RNF168* sh (TRCN0000034137: 5′-GCAGTCAGTTAATAGAAGAAA-3′), *REV3* sh (TRCN0000244436: 5′-TGACCTGTCTGAGACTATTTA-3′), *RAD51* sh (TRCN0000018879: 5′-CGGTCAGAGATCATACAGATT-3′).

For knockdown of *Ctip* and *Exo1* TRF2ts MEFs were transduced as before[11] with pRetroSuper-blas shRNA retroviruses containing the following target sequences: *Ctip* sh1: 5′-GCAAGGTTTACAAGTCAAAGT-3′, *Ctip* sh2: 5′-GCAGACCTTTCTCAGTATA-3′, *Ctip* sh3: 5′-GCATTAACCGGCTACGAAA-3′, *Exo1* sh1: 5′-GCATTTGGCACAAGAATTA-3′. Retroviral shRNAs used for knockdown of *Rnf8*, *Lig4* or *TRF2* have been described before[11]. The *53bp1* shRNA vector used in CSR assays was obtained from Origene (FI334760) and contained the following target sequence: 5′-GGAAGTTGAAACCAGTGTGATTAGTATTG-3′.

For localization and complementation experiments human *MAD2L2* complementary DNA was Gateway-cloned (Invitrogen) into pMSCV-retroviral vectors containing coding sequences for amino-terminal Flag or GFP epitopes. MAD2L2 deletion constructs were generated through Gateway-cloning (Invitrogen). The target sequences of *Mad2l2* sh4 or the human *MAD2L2* shRNA were changed to 5′-GATTTTTCAGAAACGCAAGAA-3′ or 5′-TCCCGAACTGAATCAGTATAT-3′, respectively, to create RNAi-resistant epitope-tagged MAD2L2^{RR} in pMSCV. GFP–RIF1, Flag–53BP1-DB and PTIP–GFP expression vectors were described before[23,24]. The target sequence of the human *RIF1* shRNA was changed to 5′-GCAGCGAAGTTGAAACTTGAA-3′ to create RNAi-resistant GFP–RIF1.

Quantitative real-time PCR. RNA was isolated using TRIzol reagent (Ambion) and reverse transcribed into cDNA using AMV first-strand cDNA synthesis kit for RT–PCR (Roche) according to the manufacturer's instructions. Quantitative real-time PCR (qRT–PCR) on cDNA was performed in triplicate using Power SYBR Green PCR Master Mix (Applied Biosystems) on the StepOnePlus real-time PCR system.

The following primers were used: for mouse *Mad2l2* forward 5′-ACACTCCACTGCGTCAAACC-3′ and reverse 5′-AAAGACAAACTTCTCCACTGGGC-3′; for human *MAD2L2* forward 5′-CGAGTTCCTGGAGGTGGCTGTGCATC-3′ and reverse 5′-CTTGACGCAGTGCAGCGTGTCCTGGATA-3′; for human *RNF8* forward 5′-TGGAAGAGCTAAATCGCAGCA-3′ and reverse 5′- TCAAGGTGACAGCCTCAATGAA-3′; for human *RNF168* forward 5′-GGCGAGTTTATGCTGTCCCT-3′ and reverse 5′- GCCGCCACCTTGCTTATTTC-3′; for mouse *Rev1* forward 5′-AAGCCAGATGGTCAGTACCACC-3′ and reverse 5′-TCCATTGAACGTCCAACTCCCG-3′; for human *REV3* forward 5′-AGGACTCGAAGTCACCTATGC-3′ and reverse 5′-AGAGGTAACCCCAGGAATGC-3′; for mouse *Ctip* forward 5′-GTGCTGGGTCGGAGCAG-3′ and reverse 5′-TTGACTTGTAAACCTTGCACTTCC-3′; for mouse *Exo1* forward 5′-TAAACACGTCGAGCCTGTCC-3′ and reverse 5′-CAGAGCCCAGGAACCTTGTT-3′; for human *RAD51* forward 5′-GTGGAGCTAATGGCAATGCAG-3′ and reverse 5′-TTAGCTCCTTCTTTGGCGCA-3′; for mouse *Hprt* forward 5′-CTGGTGAAAGGACCTCTCG-3′ and reverse 5′-TGAAGTACTCATTATAGTCAAGGGCA-3′; for human *GAPDH* forward 5′-GAAGGTGAAGGTCGGAGTC-3′ and reverse 5′-GAAGATGGTGATGGGATTTC-3′.

Immunoblotting. Whole-cell lysates were prepared by scraping cells in SDS sample buffer; protein concentration was determined by standard BCA protein assay (Pierce) and equal amounts of protein were separated on precast 4–12% Bis-Tris or 3–8% Tris-acetate gels (Invitrogen). Immunoblotting was done according to standard methods using IRDye800CW- and IRDye680-labelled secondary antibodies for detection on the Odyssey Infrared imager (LI-COR) or using horseradish peroxidase (HRP)-conjugated secondary antibodies for detection by enhanced chemiluminescence (Supersignal, Thermo Scientific). Primary antibodies used were against MAD2L2 (sc135977, Santa Cruz, 1:500), phospho-ATM S1981 (4526, Cell Signaling, 1:1,000), phospho-KAP1 S824 (Bethyl, 1:1,000), 53BP1 (NB100-305, Novus,

1:500), phospho-H2AX S139 (clone JBW301, Upstate, 1:1,000), CHK2 (611570, BD, 1:1,000), phospho-CHK1 S345 (2348, Cell Signaling, 1:1,000), phospho-ATR S428 (Cell Signaling, 1:1,000); RPA34 (RPA34-20, Gene Tex, 1:1,000); phospho-RPA32 S4/S8 (A300-245A, Bethyl, 1:1,000); CTIP (sc22838, Santa Cruz, 1:500); γ-tubulin (GTU-88, Sigma, 1:5,000); β-catenin (610154, BD Biosciences, 1:2,000); GFP (a-11122, Invitrogen, 1:500); RIF1 (sc55979, Santa Cruz, 1:1,000); PTIP (ABE69, Millipore and ab2614, Abcam, 1:500); actin (CP01, Calbiochem, 1:5,000). Immunoblotting for tubulin, β-catenin or actin served as loading controls.

Immunofluorescence. For immunofluorescence, cells were grown on 8-well chamber slides (Lab-Tek) and in cases of MAD2L2 detection first pre-extracted for 30 s to 5 min with 0.5% Triton/PBS on ice, then fixed for 10 min in 4% paraformaldehyde in PBS. Cells were permeabilized for 5 min (MEFs) or 10 min (U2OS) in 0.5% Triton/PBS, washed twice in PBS, incubated for 1 h in blocking solution (0.02% Triton, 5% NGS, 5% FCS in PBS) and overnight at 4 °C with primary antibodies in blocking solution. Immunofluorescence for PTIP–GFP in U2OS was done as described[24]. Primary antibodies used were against phospho-ATM S1981 (4526, Cell Signaling, 1:1,000), phospho-H2AX Ser 139 (05-636, Millipore and 2577S, Cell Signaling, 1:500), 53BP1 (A300-272A, Bethyl, 1:2,000), mRIF1 (gift from R. Chapman, 1:500)[22], RIF1 (A300-569A, Bethyl, 1:1,000), MAD2L2 (sc135977, Santa Cruz, 1:100), Flag (F3165 or F1804 at 1:500, F7425 at 1:400, Sigma), GFP (a-11122, Invitrogen, 1:500). Cells were washed three times with 0.02% Triton/PBS, followed by incubation with Alexa Fluor 488 or 568 goat anti-mouse or anti-rabbit IgG secondary antibodies (Invitrogen) in blocking solution for 1 h. After four washes in 0.02% Triton/PBS, slides were mounted in Vectashield (Vector Laboratories) containing DAPI. Confocal fluorescence images were obtained on a Leica SP5 confocal system equipped with an Ar, Kr and HeNe laser system. Images were taken with a ×63 NA 1.32 oil objective and standard LAS-AF software. Possible crosstalk between fluorochromes was avoided by careful selection of imaging conditions. A minimum of 100 cells per condition per experiment was analysed. DDR foci in MEFs were captured using the Metafer4/MetaCyte platform (MetaSystems) equipped with an AxioImager Z2 microscope (Carl Zeiss). Images of random selections of cells were acquired with an EC 'Plan-Neofluar' ×40/0.75 objective. Analysis was done using MetaCyte software, carefully fine-tuned for each antibody. A minimum of 500 cells was analysed per condition per experiment for p-ATM, γH2AX, 53BP1 and RIF1. All assessments of irradation-induced DDR foci were done 3 h after irradiation with 5 Gy, with the exception of Fig. 3a, which is 30 min after 10 Gy.

Metaphase chromosome analysis. Cell collection, preparation of metaphase spreads and telomere FISH with a FITC-OO-$(CCCTAA)_3$ peptide nucleic acid custom probe (Biosynthesis) for metaphase chromosome analysis was done as described[5].

Digital images of metaphases were captured using the Metafer4/MSearch automated metaphase finder system (MetaSystems) equipped with an AxioImager Z2 microscope (Carl Zeiss). After scanning metaphase preparations at ×10 magnification, high-resolution images of metaphases were acquired using a 'Plan-Apochromat' ×63/1.40 oil objective. Chromosome fusions were quantified from >30 metaphases.

For monitoring mitotic telomeres by PNA FISH, IMR90 (E6/E7) cells were transduced with pMX-Flag-53BP1 (1-1711) or its mutant Thr1608Ala/Ser1618Ala (TASA) and pMX-GFP-RNF8 or its mutant Thr198Ala and selected with 0.2 μg ml^{-1} puromycin, for 3 days before plating. Cells were transfected with siRNAs targeting endogenous RNF8 (ThermoFisher, D-006900-01, target sequence: 5′-AGAAUG AGCUCCAAUGUAUUU-3′) and 53BP1 (ThermoFisher, D-003548-01, target sequence: 5′-GAGAGCAGAUGAUCCUUUA-3′) and the following siRNAs: PTIP siRNA pool (ThermoFisher, D-012795-01-0010, target sequences: 5′-UUAAAG CGAGCAAGUAUUA-3′, 5′-GAGCCUGGGUUGAUUAACU-3′, 5′-GUUGA UGAGUAUAAGACUA-3′ and 59-GCCAAUGCAGUGCUGUUUA-3′), RIF1 (ThermoFisher, D-027983-02, target sequence: 5′-AGACGGUGCUCUAUUGU UA-3′), MAD2L2 (ThermoFisher, D-003272-10: 5′-GAGAAAUUCGUCUUUG AGA-3′) and non-targeting control siRNA (ThermoFisher, D-001210-02, target sequence: 5′-UAAGGCUAUGAAGAGAUAC-3′) using RNAiMax (Invitrogen) and synchronized with a double-thymidine block. Cells were subsequently processed as previously described[16].

Pulsed-field gel electrophoresis and in-gel detection of telomeric DNA. Analysis of 3′ single-stranded G-overhangs at mouse telomeres was performed as described[5] by pulsed-field gel electrophoresis and in-gel hybridization of a ^{32}P-labelled telomeric repeat $(CCCTAA)_4$ oligonucleotide to native DNA. In brief, *Trf2*$^{-/-}$ *p53*$^{-/-}$ TRF2ts MEFs were collected at the permissive temperature as well as after growth at the non-permissive temperature. Agarose plugs were prepared containing 1×10^6 cells per plug and digested overnight with 1 mg ml^{-1} proteinase K at 50 °C. Before loading on a 1% agarose gel, plugs were digested overnight with 60 U of MboI enzyme per plug. After running the gel on a CHEF-DR III pulsed-field gel electrophoresis system (BioRad), the gel was dried, pre-hybridized in Church Mix containing 7% SDS and hybridized overnight with a ^{32}P-labelled $(CCCTAA)_4$ probe, all under non-denaturing conditions. Signal was captured on a phosphorimager and analysed with AIDA Image Analyzer software. To confirm that the G-overhang signal detected with this method was indeed derived from 3′ single-stranded telomeric TTAGGG repeats, digestion with 3′ exonuclease and hybridization with a ^{32}P-labelled $(TTAGGG)_4$ probe specific for the C-rich strand was performed on separate plugs. After capturing the hybridization signal from single-stranded telomeric DNA, the gel was denatured and re-hybridized with the same probes to obtain a total telomere signal for the purpose of quantification.

Repair and clonogenic survival assays. To quantify the repair of DSBs by NHEJ, U2OS cells transduced with shRNAs were transfected with pEJ5-GFP (NHEJ), as well as an mCherry expression vector and pCAGGS-Isce-I-Trex2 (ref. 30). Transfections were done using Mirus TransIT LT-1 (Mirus Bio LLC). The fraction of mCherry-positive cells that was GFP-positive was determined 72 h after transfection by flow-cytometry on a BD LSRFortessa using FACSDiva software. Quantification was carried out with FlowJo software (TreeStar).

For random plasmid integration assays 500,000 U2OS cells were seeded in 6-cm dishes 24 h before transfection with 3.9 μg of NdeI-linearized pMSCVblas-GFP and 0.1 μg of mCherry plasmids using ViaFect (Promega). Transfected cells were trypsinized the following day and seeded in 10-cm dishes at different densities for colony formation. Selection was initiated the following day with blasticidin at 5 μg ml^{-1}. Cells were fixed with 4% paraformaldehyde 10–14 days after plating and stained with 0.1% crystal violet. Colony counting was performed on a ColCount (Oxford Optronix) and values were normalized for plating and transfection efficiencies.

For clonogenic survival assays U2OS cells were seeded in duplicate in 6-well plates at 100, 200 and 400 cells per well for unirradiated cells, and at 400, 800 and 1,600 cells per well for irradiated cells. Cells were grown for <20 h before γ-irradiation and then fixed after 10–12 days of recovery with 4% paraformaldehyde and stained with 0.1% crystal violet. Colonies with >50 cells were counted on a GelCount (Oxford Optronix) and the surviving fraction was determined.

CSR assays. Research involving animals was performed in accordance with protocols approved by the animal facility at Toronto Centre for Phenogenomics (Toronto). Primary B cell extraction was performed as described before[23]. In brief, mature B lymphocytes were isolated from spleens of 8–12-week-old C57BL/6 mice by depletion of CD43$^+$ cells using CD43 microbeads (Miltenyi Biotech) according to the manufacturer's instructions. Purified B cells were resuspended at a concentration of 10^6 cells per ml in the presence of 25 μg ml^{-1} LPS (Sigma-Aldrich) to allow B cell proliferation. Both mouse CH12F3-2 (ref. 31) and primary B cells were infected with lentiviral/retroviral particles obtained from the supernatant of HEK293T cell cultures cotransfected with the lentiviral/retroviral shRNA constructs and the vector expressing MLV Gag-Pol (for retrovirus) or the lentiviral psPAX2 packaging vector with VSV-G envelope (2:1:1 ratio). In brief, the viral supernatant was concentrated at 25,000*g* for 90 min at 25 °C before resuspension in RPMI culture medium. Infection was subsequently performed as described[23] and followed by selection with puromycin.

IgM to IgA switching was assayed in CH12F3-2 cells activated with 1 ng ml^{-1} TGF-β1 (Preprotech), 10 ng ml^{-1} IL-4 (Preprotech) and 1 μg ml^{-1} agonist anti-CD40 (BD). IgA expression was measured by flow-cytometry using biotin-conjugated anti-mouse IgA antibody (1:200; eBioscience) followed by an anti-biotin-APC antibody at 0, 24 and 48 h after activation. Proliferation of the different transduced CH12F3-2 cell lines was monitored using CFSE (Invitrogen) following the manufacturer's guidelines. CSR assays in both cell types were done in triplicate for every independent experiment.

Ex-vivo isotype switching to IgG1 in primary B cells was assayed by flow-cytometry using an anti-IgG1-biotin (1:200; BD) followed by allophycocyanin (APC)-conjugated anti-biotin (Miltenyi Biotech) and 10 μg ml^{-1} propidium iodide 5 days after isolation.

For semiquantitative RT–PCR analysis of *Aid* mRNA, IgM and IgA germ-line transcripts total RNA was extracted with TRIzol (Invitrogen) and cDNA was synthesized by random priming using the Superscript III reverse transcriptase kit (Invitrogen). Mouse *Aicda* transcripts were amplified using oligonucleotides 5′-G TGCCACCTCCTGCTCACTGG-3′ and 5′-TTCATGTAGCCCTTCCCAGGC-3′. IgM (μ) germ-line transcripts were amplified using oligonucleotides 5′-AAAATG TCCGCTGGGCTAAG-3′ and 5′-AGAACAGTCCAGTGTAGGCAGTAGA-3′, IgA (Iα) using 5′-CCTGGCTGTTCCCCTATGAA-3′ and 5′-GAGCTGGTGGG AGTGTCAGTG-3′; and *Gapdh* transcripts were amplified using oligonucleotides 5′-AGCCTCGTCCCGTAGACAA-3′ and 5′-AATCTCCACTTTGCCACTGC-3′. 53BP1 depletion is known to impair CSR[3] and was included as control.

TSCE. TSCE were detected by chromosome-orientation FISH, essentially as described[32] with minor modifications. In brief, for chromosome-orientation FISH cells were grown in 10 μM BrdU:BrdC (3:1) for 24 h with the addition of 0.2 μg ml^{-1} demecolcine for the final 2 h. Slides were treated with RNase A (0.5 mg ml^{-1}) for 10 min at 37 °C, stained with Hoechst 33258 (0.5 μg ml^{-1}) in 2× SSC for 15 min at room temperature and exposed to 5.4×10^3 J m^{-2} 365-nm ultraviolet light

(Stratalinker 2400 UV irradiator). Following digestion with exonuclease III (10 U μl^{-1}, Promega) for 10 min at room temperature, slides were dehydrated through an ethanol series (70%, 95% and 100%) and incubated sequentially with Cy3-TelG 5′-$[TTAGGG]_3$-3′ and FITC-TelC 5′-$[CCCTAA]_3$-3′ probes at room temperature.

Telomere mobility. Telomere mobility analysis was done as described[13] with minor adjustments. TRF2ts cells expressing eGFP-TRF1 and mCherry-BP1-2 (53BP1 amino acids 1220–1711) were seeded on Willco wells and left to attach overnight at 32 °C. Before imaging, cells were incubated at 37 °C for 30 min in Leibovitz's L15 medium inside the Microscope climate chamber. Cells were monitored every minute for 20 min ($t = 20$ frames) at 37 °C. Five-micrometre *Z*-stacks at 0.5-μm steps in both eGFP and mCherry channels were obtained with a ×63 1.4 oil objective using ZEN software on an Observer Z1 microscope system (Carl Zeiss). Images were obtained at 2 × 2 binning with 512 × 512 pixels. Tracking of telomeres was performed with FIJI software, cells were registered with the Rigid body option from the StackReg plugin. Particles were then tracked with the particle detector and tracker plugin from Mosaic. Telomeres to track were selected on basis of colocalization with mCherry-BP1-2, and tracked for at least 17 out of 20 frames.

Database. To address whether changes in *MAD2L2* mRNA expression occur in human cancers we consulted the Oncomine database at https://www.oncomine.org/resource/login.html.

Statistics. No statistical methods were used to predetermine sample size. *P* values were determined by Kruskal–Wallis ANOVA test.

30. Bennardo, N., Gunn, A., Cheng, A., Hasty, P. & Stark, J. M. Limiting the persistence of a chromosome break diminishes its mutagenic potential. *PLoS Genet.* **5,** e1000683 (2009).
31. Kato, H. *et al.* Involvement of RBP-J in biological functions of mouse Notch1 and its derivatives. *Development* **124,** 4133–4141 (1997).
32. Celli, G. B., Denchi, E. L. & de Lange, T. Ku70 stimulates fusion of dysfunctional telomeres yet protects chromosome ends from homologous recombination. *Nature Cell Biol.* **8,** 885–890 (2006).

a

shRNA	Average ratio over 3 screens
TRCN0000012846:Mad2l2	43.61
TRCN0000040875:Rnf168	18.54
TRCN0000120626:Rad50	13.73
TRCN0000039432:Rnf8	11.09
TRCN0000081778:Trp53bp1	11.03
TRCN0000012646:Atm	7.39
TRCN0000039429:Rnf8	7.27
TRCN0000012645:Atm	5.60
TRCN0000120622:Rad50	4.58
TRCN0000012647:Atm	4.32
TRCN0000012672:Nbn	3.76
TRCN0000012844:Mad2l2	3.11
TRCN0000012669:Nbn	2.62
TRCN0000012671:Nbn	1.62
TRCN0000120623:Rad50	1.38

b

shRNA	Ratio >1.5 in 1 of 3 screens
TRCN0000012843:Mad2l2	223.08
TRCN0000012845:Mad2l2	2.34
TRCN0000040873:Rnf168	9.10
TRCN0000040874:Rnf168	14.50
TRCN0000040876:Rnf168	3.23
TRCN0000039433:Rnf8	1.94
TRCN0000039431:Rnf8	12.55
TRCN0000081781:Trp53bp1	2.18
TRCN0000081779:Trp53bp1	1.88
TRCN0000012644:Atm	2.47
TRCN0000012643:Atm	4.66
TRCN0000012668:Nbn	14.11
TRCN0000012670:Nbn	4.52

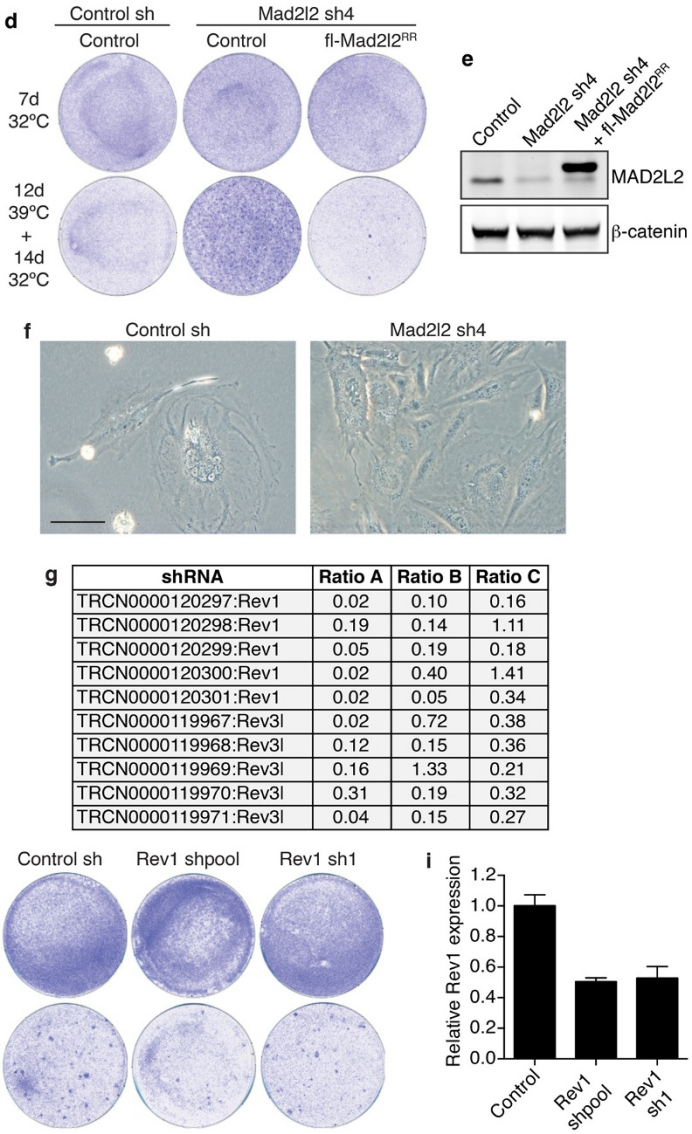

g

shRNA	Ratio A	Ratio B	Ratio C
TRCN0000120297:Rev1	0.02	0.10	0.16
TRCN0000120298:Rev1	0.19	0.14	1.11
TRCN0000120299:Rev1	0.05	0.19	0.18
TRCN0000120300:Rev1	0.02	0.40	1.41
TRCN0000120301:Rev1	0.02	0.05	0.34
TRCN0000119967:Rev3l	0.02	0.72	0.38
TRCN0000119968:Rev3l	0.12	0.15	0.36
TRCN0000119969:Rev3l	0.16	1.33	0.21
TRCN0000119970:Rev3l	0.31	0.19	0.32
TRCN0000119971:Rev3l	0.04	0.15	0.27

Extended Data Figure 1 | Related to Fig. 1. a, A functional genetic screen for TIGIRs identifies independent shRNAs against *Mad2l2* and the previously identified regulators of NHEJ-mediated telomere fusion *Atm*, *Nbs1* (also known as *Nbn*), *Rad50*, *53bp1* and *Rnf8*. Listed are the independent shRNAs enriched >1.5-fold in at least two out of three TIGIR screens, with their average ratio of enrichment over all three screens. Ratios reflect shRNA abundance after 12 days of telomere uncapping at 39 °C followed by 4 days recovery at 32 °C versus shRNA abundance after growth for 4 days at 32 °C. **b**, Additional shRNAs targeting *Mad2l2* or known TIGIRs that were enriched >1.5-fold in one out of three screens, with their ratio. Not shown are additional shRNAs against factors not previously implicated in control of telomere fusion, that were considerably enriched in these TIGIR screens but await validation. **c**, qRT–PCR analysis of *Mad2l2* expression levels in TRF2ts MEFs transduced with four independent shRNAs targeting *Mad2l2* and used in Fig. 1b (error bars denote s.d.). **d**, Survival assay of TRF2ts cells infected with control or *Mad2l2* sh4 shRNAs, complemented with empty control or RNAi-resistant Flag-MAD2L2^{RR} and grown as indicated. **e**, Western blot showing expression of endogenous MAD2L2 and exogenous Flag–MAD2L2 in TRF2ts cells used in **d** and in Fig. 1c. **f**, Photograph of shRNA-transduced TRF2ts cells grown for 12 days at 39 °C. Scale bar, 100 μm. **g**, None out of ten shRNAs targeting *Rev1* or *Rev3* were substantially enriched in any of three independent DDR TIGIR screens. **h**, shRNA-mediated *Rev1* knockdown does not increase survival after prolonged telomere uncapping in survival assays of TRF2ts MEFs. Of note, *Rev3* knockdown compromised viability and was therefore not informative in these assays. **i**, qRT–PCR analysis of mouse *Rev1* expression levels of cells shown in **h** (error bars denote s.d.).

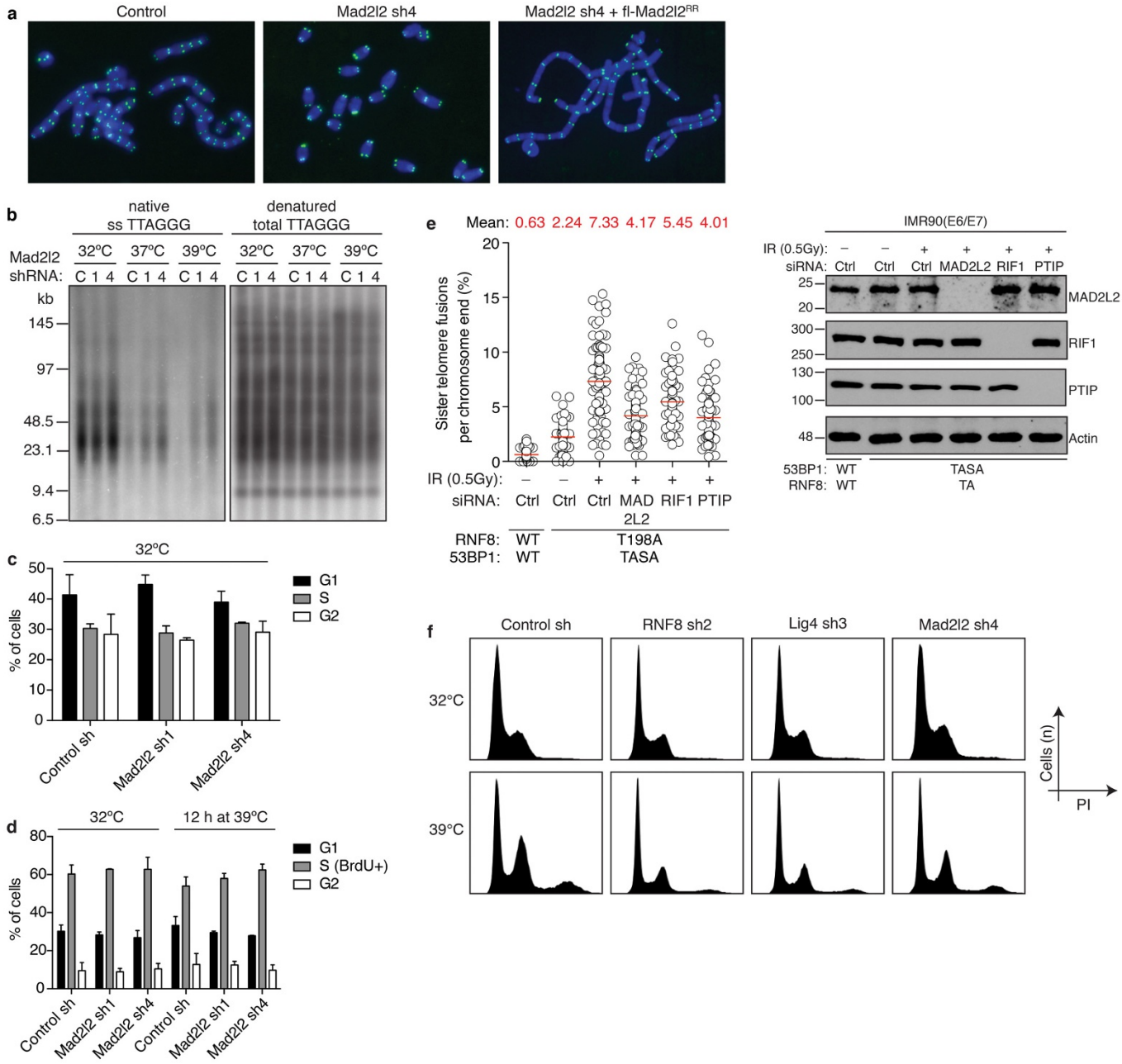

Extended Data Figure 2 | Related to Fig. 2. **a**, Representative metaphase spreads of TRF2ts MEFs transduced as indicated, collected after 24 h at 39 °C for telomere FISH. Original magnifications, ×63. **b**, Representative telomeric single-stranded G-overhang (ss TTAGGG) and total telomere (total TTAGGG) analysis in TRF2ts MEFs at 32 °C and after 48 h at 37 °C or 39 °C. **c**, **d**, *Mad2l2* knockdown does not affect cell cycle parameters in TRF2ts MEFs. Cell cycle phase analysis was based on propidium iodide staining of asynchronously growing cells (**c**), as well as on 1 h incubation with BrdU, followed by detection of BrdU incorporation and propidium iodide staining for DNA content (**d**) ($n = 3$, mean ± s.d.). **e**, MAD2L2 is required for sister-telomere fusion upon activation of DNA repair in mitosis. Sister-telomere fusions were quantified in IMR90 cells expressing exogenous wild-type 53BP1 and RNF8, or 53BP1 (Thr1608Ala/Ser1618Ala) (TASA) and RNF8(Thr198Ala) (TA) mutant alleles, and depleted for endogenous RNF8 and 53BP1, as well as depleted for MAD2L2, RIF1 or PTIP ($n = 4$). **f**, Examples of DNA content profiles of TRF2ts cells transduced with the indicated shRNAs, grown at 32 °C, or for 48 h at 39 °C and stained with propidium iodide. Analysis of the fraction of cells with 8*N* (tetraploid) or >4*N* (aneuploid) DNA content was done on corresponding dotplots of which the results are shown in Fig. 2c.

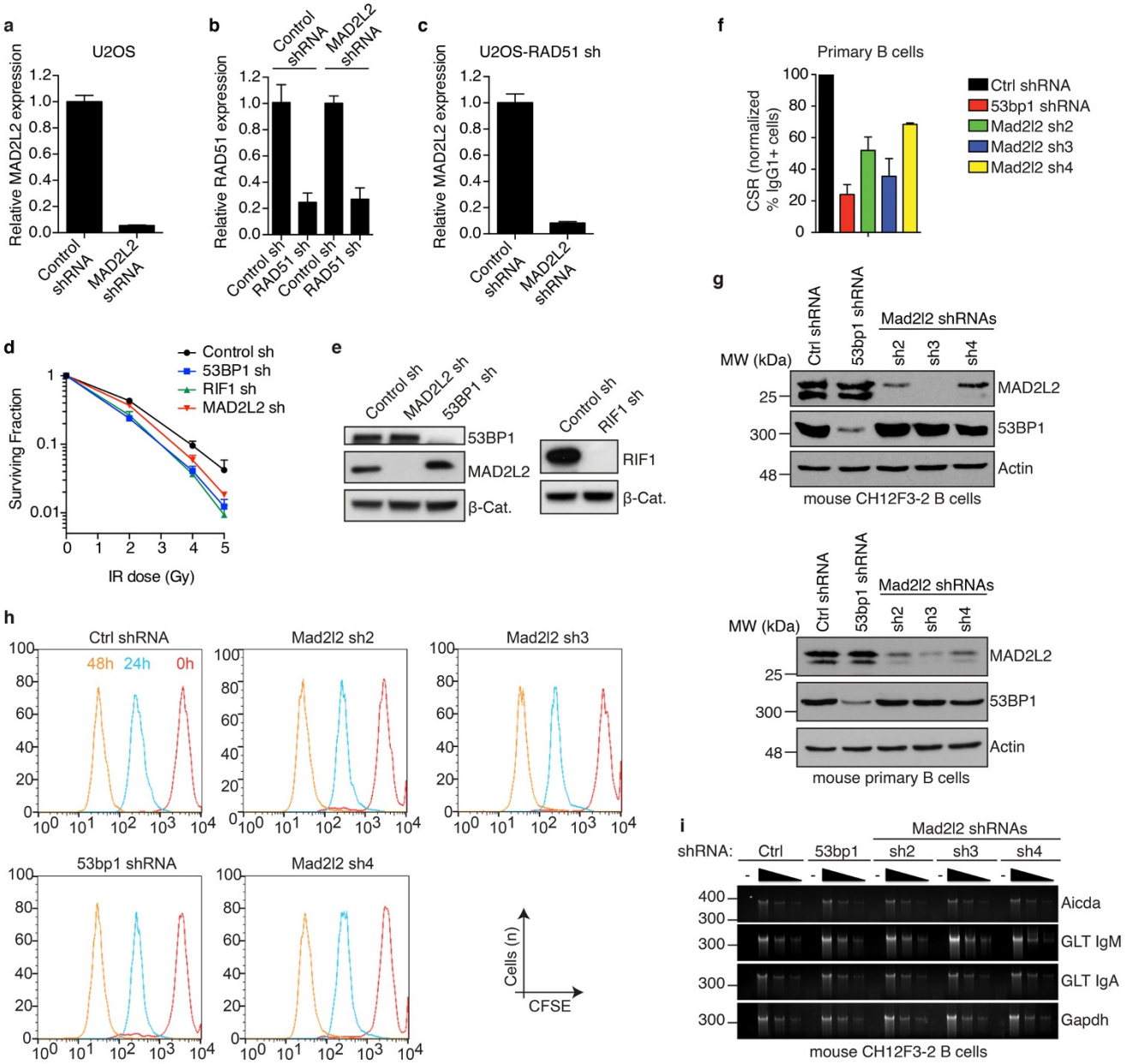

Extended Data Figure 3 | Related to Fig. 2. **a**, qRT–PCR analysis of *MAD2L2* expression levels in U2OS cells infected with control or *MAD2L2* shRNAs, and used in the repair assays shown in Fig. 2d (error bars denote s.d.). **b**, **c**, qRT–PCR analysis of *RAD51* (**b**) and *MAD2L2* (**c**) expression levels in RAD51-depleted, E6E7-expressing U2OS cells used in the assays shown in Fig. 2e (error bars denote s.d.). **d**, Clonogenic survival assays of U2OS cells transduced with non-targeting control or *53BP1*, *RIF1* or *MAD2L2* shRNAs and treated with the indicated doses of ionizing radiation ($n = 3$–4, mean ± s.e.m.). **e**, Western blot analysis of 53BP1, MAD2L2 and RIF1 in U2OS cells transduced with the indicated shRNAs. **f**, CSR in shRNA-transduced primary B cells ($n = 2$, mean ± s.d.). **g**, Western blot analysis of MAD2L2 and 53BP1 in CH12F3-2 B cells and mouse primary B cells transduced with the indicated shRNAs. **h**, MAD2L2 depletion does not affect cellular proliferation in murine B cells. CH12F3-2 cells transduced with control, *53bp1* or *Mad2l2* shRNAs were loaded with CFSE and analysed by flow cytometry at 0, 24 and 48 h after stimulation. Profiles from all time points are plotted in the same histogram. **i**, MAD2L2 depletion does not affect the transcription of critical genes implicated in CSR. RT–PCR analysis of *Aid* (*Aicda*) mRNA, IgM and IgA germline transcript (GLT) levels using twofold serial dilutions of cDNA made from activated CH12F3-2 B cells transduced with the indicated shRNAs. *Gapdh* was used as a control for transcript expression.

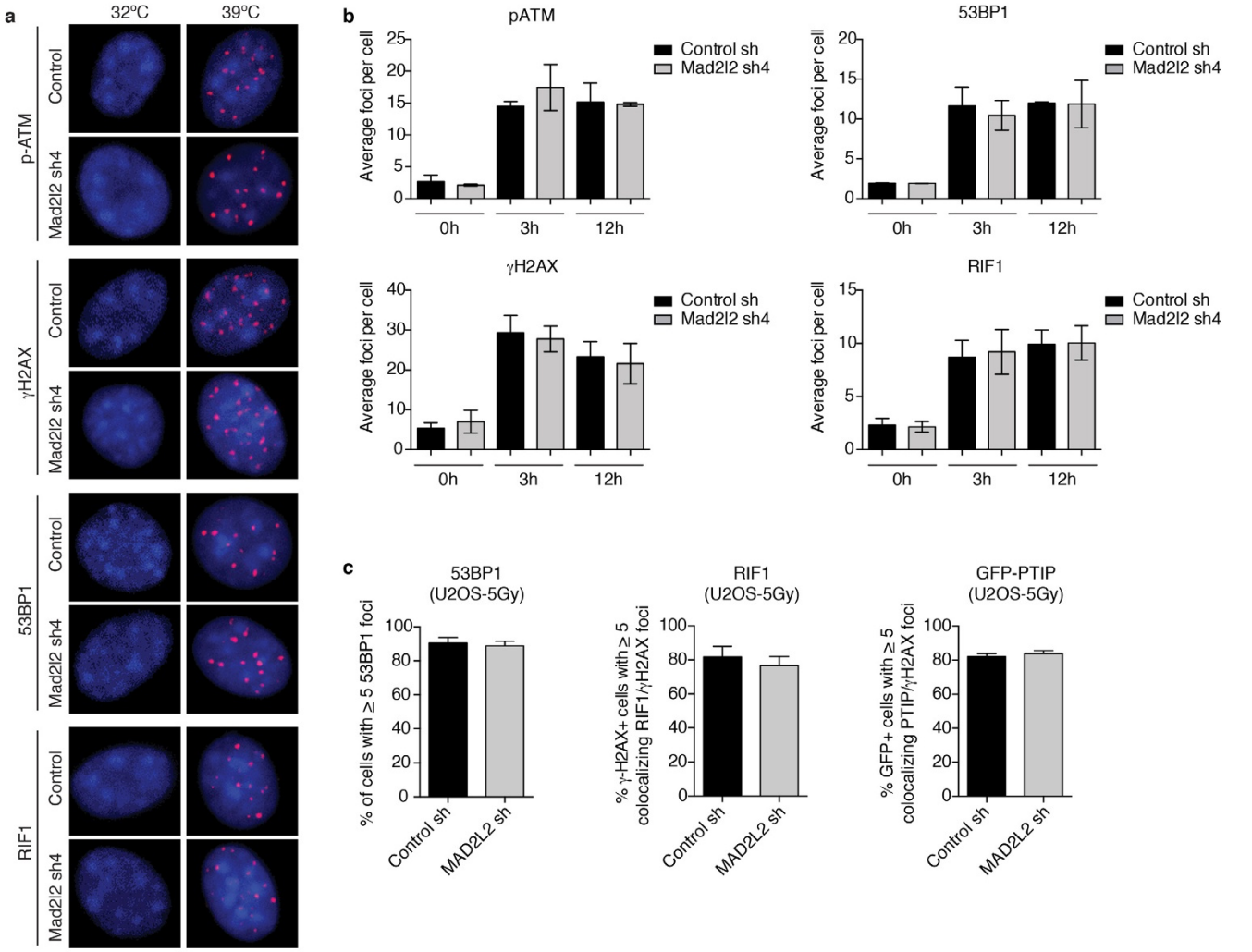

Extended Data Figure 4 | Related to Fig. 3. **a**, Representative images of immunofluorescence detection of p-ATM(S1981), γH2AX, 53BP1 and RIF1 in TRF2ts MEFs transduced with control or *Mad2l2* shRNAs and grown at 32 °C or for 12 h at 39 °C to induce telomere uncapping. DNA was stained with 4',6-diamidino-2-phenylindole (DAPI). Original magnifications, ×40. **b**, Quantification of the number of p-ATM, γH2AX, 53BP1 and RIF1 foci per cell in TRF2ts MEFs transduced with control or *Mad2l2* shRNAs and grown at 32 °C or for 3 and 12 h at 39 °C ($n = 2$, mean ± s.d.). **c**, Quantifications of 53BP1, RIF1 and PTIP foci in U2OS cells transduced with control or *MAD2L2* shRNAs, 3 h after 5 Gy ($n = 2$, mean ± s.d.).

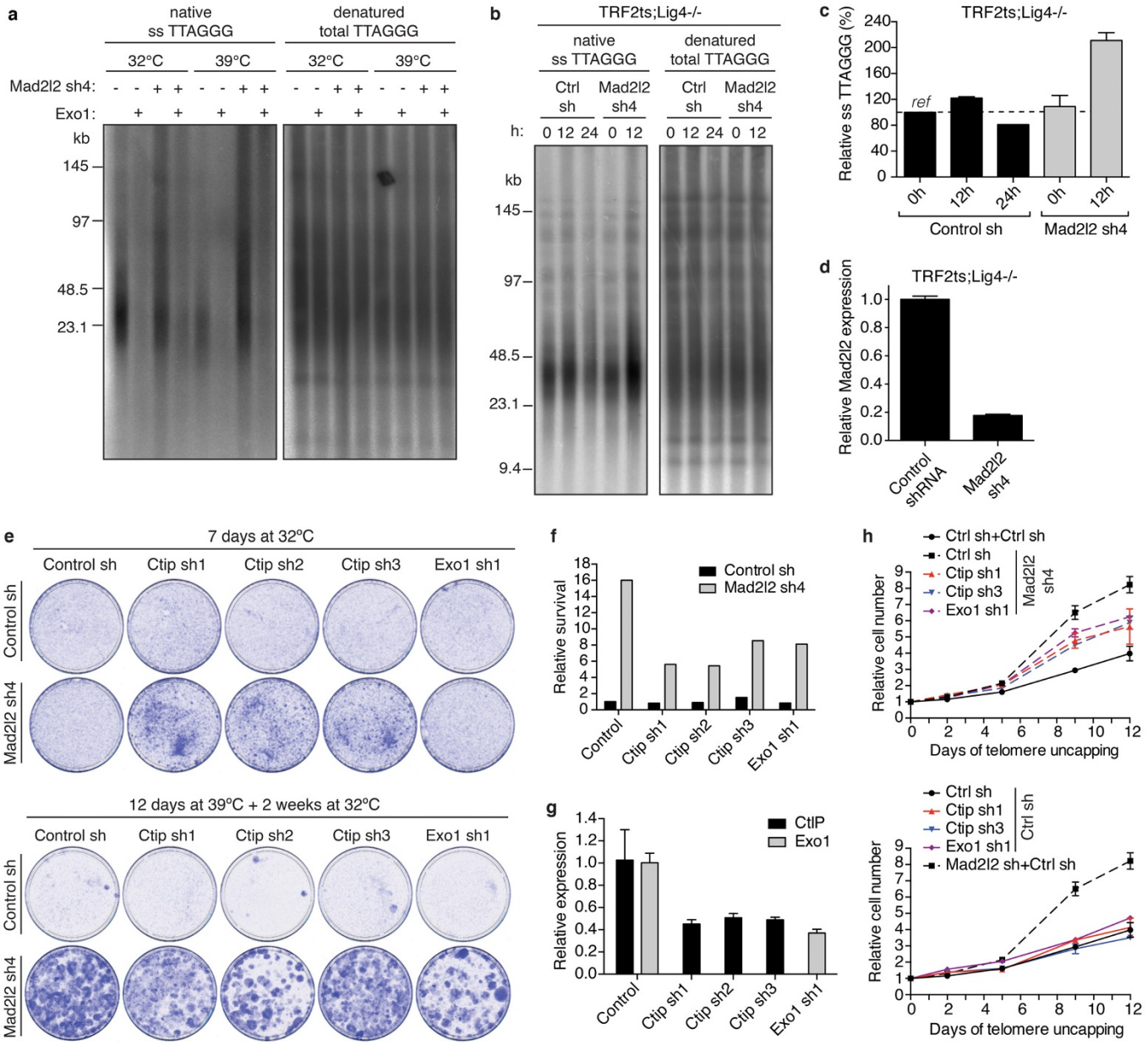

Extended Data Figure 5 | Related to Fig. 3. **a**, Telomeric single-stranded G-overhang assay of TRF2ts MEFs transduced with control or *Mad2l2* sh4 shRNAs, showing that the increase in overhang signal upon *Mad2l2* knockdown is due to 3′ terminal sequences because the signal is removed by treatment with *Escherichia coli* 3′ exonuclease Exo1. **b**, *Mad2l2* knockdown causes increased single-stranded telomeric G-overhang signals in TRF2ts *Lig4*$^{-/-}$ MEFs. **c**, Quantification of relative telomeric G-overhang signals in TRF2ts *Lig4*$^{-/-}$ MEFs transduced with control or *Mad2l2* shRNAs and grown at 32 °C or for 12 or 24 h at 39 °C ($n = 2$, mean ± s.e.m.). **d**, qRT–PCR analysis of *Mad2l2* expression levels in TRF2ts *Lig4*$^{-/-}$ MEFs infected with control or *Mad2l2* shRNA lentivirus (error bars denote s.d.). **e**, Survival assays of TRF2ts MEFs transduced with control or *Mad2l2* shRNAs and subsequently with control, *Ctip* or *Exo1* shRNAs. **f**, Quantification of the survival assays shown in **e**. **g**, qRT–PCR analysis of *Ctip* and *Exo1* expression levels of cells shown in **e**, **f** and **h** and in Fig. 3f (error bars denote s.d.). **h**, Growth curves at 39 °C of TRF2ts MEFs transduced with non-targeting control or *Mad2l2* shRNAs and subsequently with control, *Ctip* or *Exo1* shRNAs (error bars denote s.e.m.).

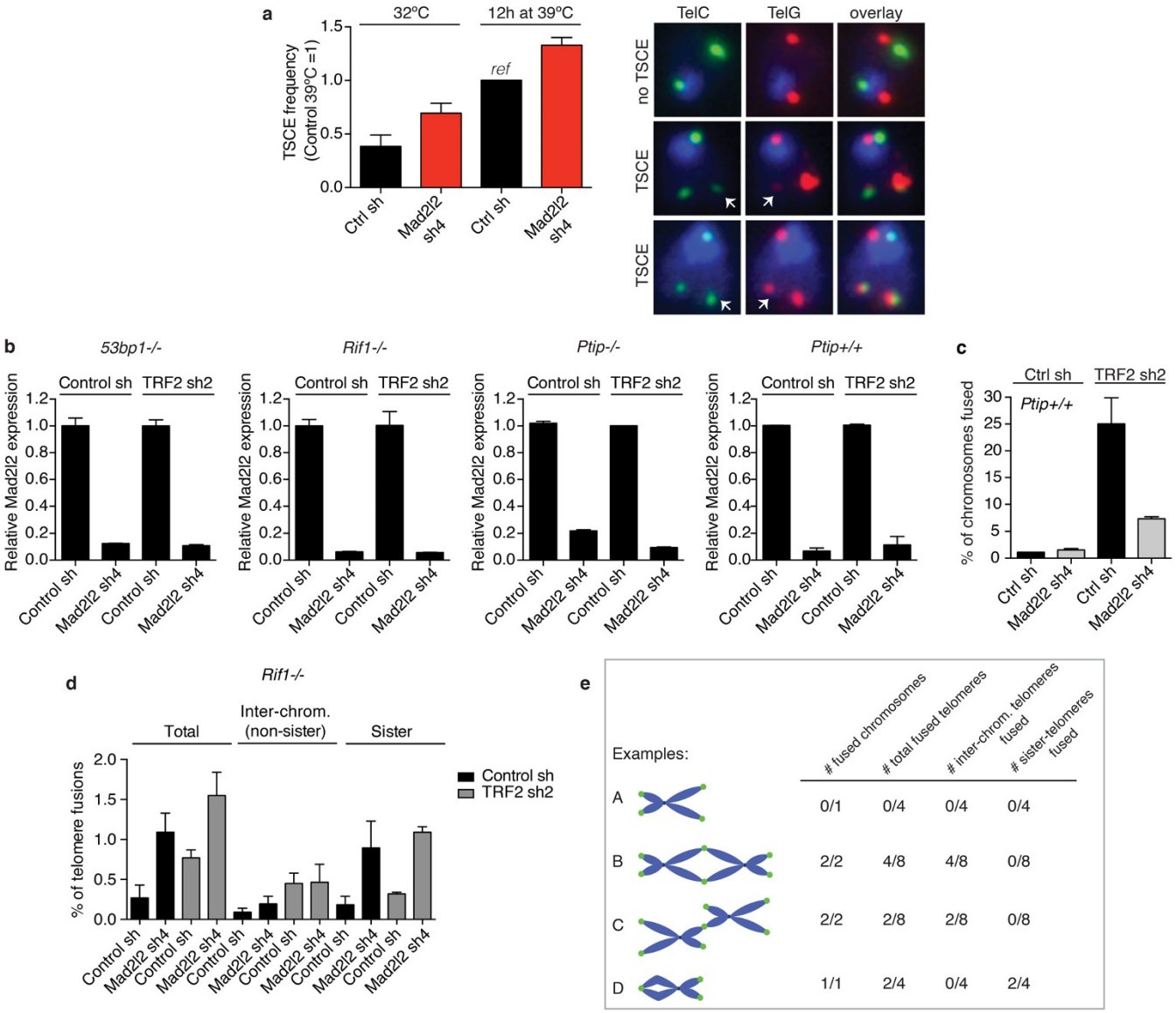

Extended Data Figure 6 | Related to Figs 3 and 4. **a**, TSCE analysis in shRNA-transduced TRF2ts MEFs grown at 32 °C or for 12 h at 39 °C to uncap telomeres ($n = 2$, mean ± s.d., counting >1,000 chromosomes per condition, per experiment). TSCE frequency in control cells is set at 1 (corresponding to an average of 6.9% of chromosomes with a TSCE event). Shown on the right are examples of chromosomes without and with TSCE in cells quantified on the left. Original magnifications, ×63. **b**, qRT–PCR analysis of *Mad2l2* expression levels in *53bp1*$^{-/-}$, *Rif1*$^{-/-}$, *Ptip*$^{-/-}$ and *Ptip*$^{+/+}$ MEFs used in the chromosome fusion analysis shown in Fig. 4a and in **c** (error bars denote s.d.). **c**, Percentage of chromosomes fused upon TRF2 inhibition in the *Ptip*$^{+/+}$ MEFs matching with the *Ptip*$^{-/-}$ MEFs shown in Fig. 4a ($n = 2$, mean ± s.e.m.). **d**, Analysis of different types of telomere fusions in *Rif1*$^{-/-}$ MEFs. Depletion of MAD2L2 in *Rif1*$^{-/-}$ MEFs does not reduce inter-chromosomal telomere fusions induced by TRF2 inhibition, indicating epistasis. However, irrespective of TRF2 inhibition, MAD2L2 depletion in *Rif1*$^{-/-}$ MEFs induces association between sister telomeres, causing an increase in total fusions scored for MAD2L2-depleted *Rif1*$^{-/-}$ MEFs, as also visible in Fig. 4a ($n = 2$, mean ± s.e.m., >1,300–2,000 chromosomes were analysed per condition, per independent experiment). **e**, Explanation of scoring different types of telomere fusions shown in **d**.

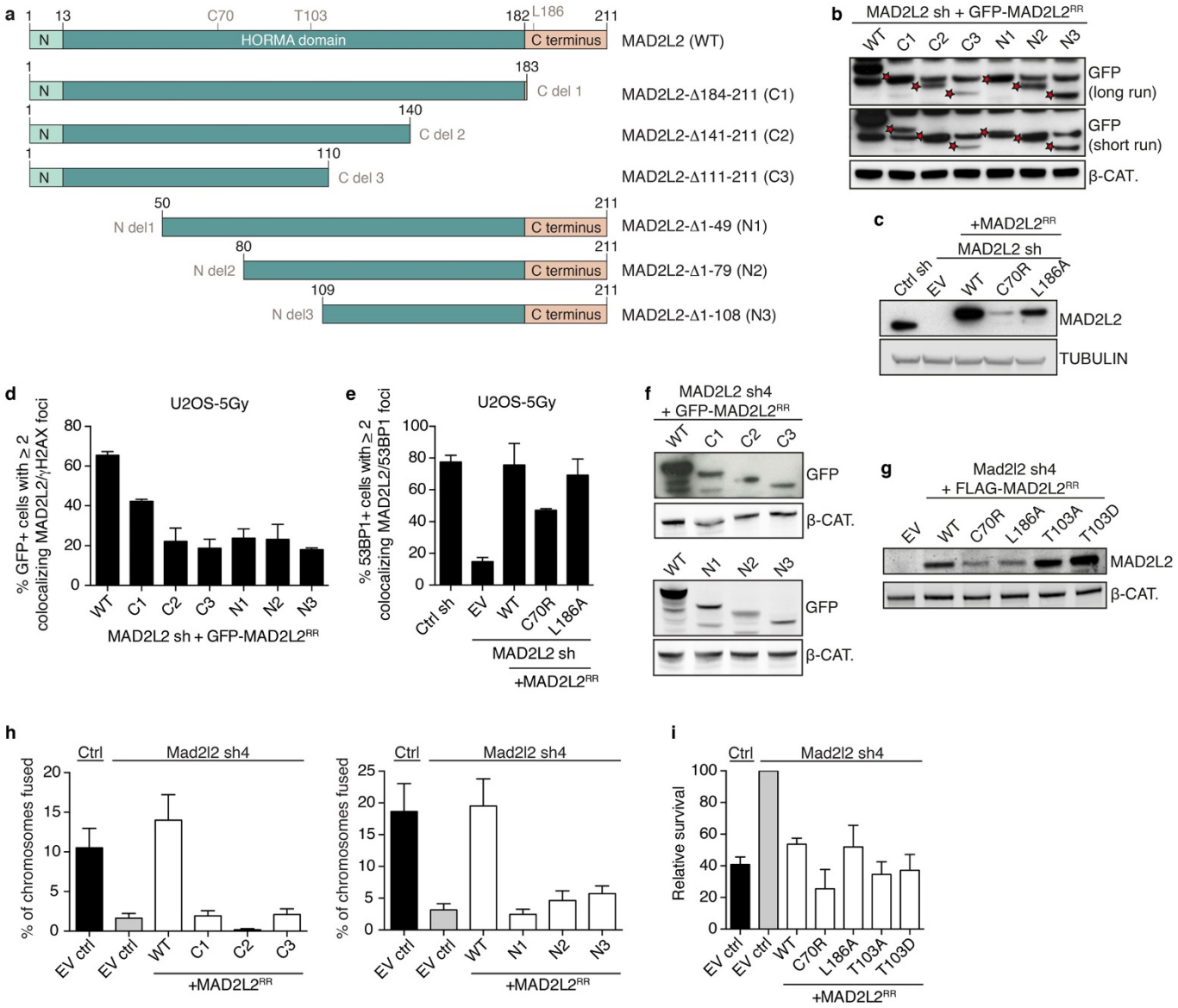

Extended Data Figure 7 | Related to Fig. 4. **a**, Schematic overview of C-terminal and N-terminal deletion mutants of MAD2L2. **b**, **c**, Expression analysis in U2OS cells of GFP-tagged wild-type MAD2L2 and C- and N-terminal MAD2L2 deletion mutants (**b**) and of Flag-tagged wild-type MAD2L2 and MAD2L2(Cys70Arg) and MAD2L2(Leu186Ala) (**c**). **d**, Analysis of DDR foci formation of GFP-tagged wild-type MAD2L2 and C- and N-terminal MAD2L2 deletion mutants by immunofluorescence detection of GFP and γH2AX in U2OS at 3 h after ionizing radiation ($n = 2$ for N-terminals, $n = 3$ for C-terminals, mean ± s.e.m.). **e**, Analysis of wild-type, Cys70Arg and Leu186Ala MAD2L2 accumulation into DDR foci by immunofluorescence detection of MAD2L2 and 53BP1 in U2OS at 3 h after ionizing radiation ($n = 2$, ± s.e.m.). **f**, **g**, Expression analysis in TRF2ts MEFs of GFP-tagged MAD2L2 and C- and N-terminal MAD2L2 deletion mutants (**f**) and of Flag-tagged wild-type MAD2L2 and MAD2L2(Cys70Arg), MAD2L2(Leu186Ala), MAD2L2(Thr103Ala) and MAD2L2(Thr103Asp) (**g**). **h**, Quantification of chromosome fusions after 24 h of telomere deprotection at 39 °C in TRF2ts MEFs transduced with control or *Mad2l2* shRNAs and complemented with empty vector control or RNAi-resistant GFP-tagged wild-type MAD2L2 and C- or N-terminal MAD2L2 deletion mutants (error bars denote s.e.m.). **i**, Quantification of survival assays of TRF2ts MEFs transduced with control or *Mad2l2* shRNAs and subsequently with empty vector control, wild-type MAD2L2, MAD2L2(Cys70Arg), MAD2L2(Leu186Ala), MAD2L2(Thr103Ala) or MAD2L2(Thr103Asp) retroviruses ($n = 2$, mean ± s.e.m.).

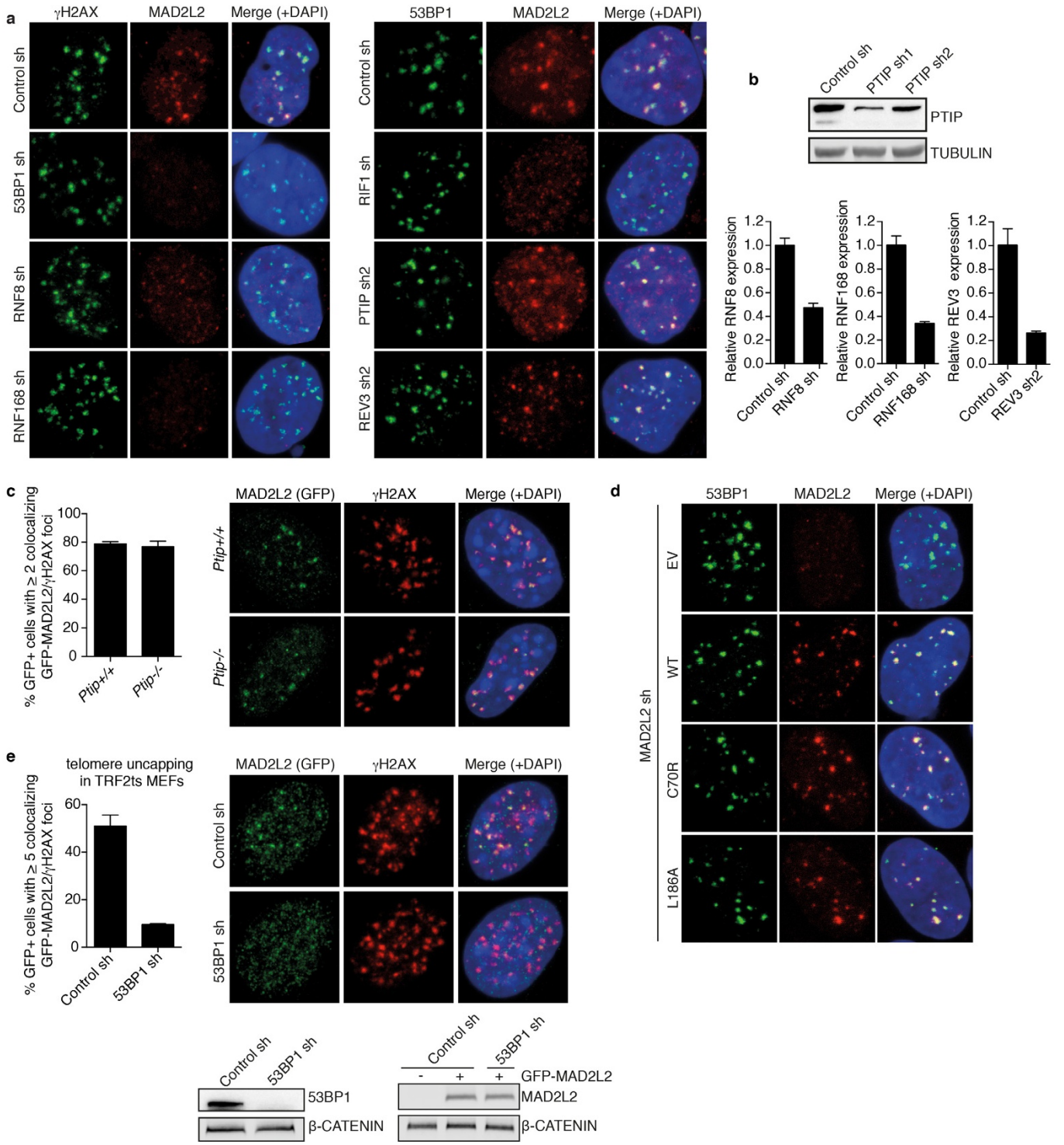

Extended Data Figure 8 | Related to Fig. 4. **a**, Representative images of immunofluorescence detection of endogenous MAD2L2 and γH2AX or 53BP1 in U2OS cells transduced with control, *53BP1*, *RNF8*, *RNF168*, *RIF1*, *PTIP* or *REV3* shRNA lentiviruses, irradiated with 5 Gy and processed for immunofluorescence after 3 h (quantifications are shown in Fig. 4e). **b**, Western blot or qRT–PCR analysis of PTIP, RNF8, RNF168 and REV3 levels in shRNA-transduced U2OS cells (error bars denote s.d.). **c**, Quantification and representative images of immunofluorescence detection of γH2AX and GFP–MAD2L2 in $Ptip^{+/+}$ or $Ptip^{-/-}$ MEFs, 3 h after 5 Gy ($n = 2$, mean ± s.d.). **d**, Representative images of immunofluorescence for 53BP1 and exogenous Flag–MAD2L2 wild-type, Cys70Arg or Leu186Ala mutants in U2OS cells depleted for endogenous MAD2L2 with lentiviral shRNA, processed for immunofluorescence 3 h after 5 Gy (quantifications are shown in Extended Data Fig. 7e). **e**, Quantification and representative immunofluorescence images of GFP–MAD2L2 localization to uncapped telomeres in TRF2ts MEFs transduced with control or *53bp1* shRNAs ($n = 2$, mean ± s.d.). Original magnifications, ×63 with zoom factor 5.

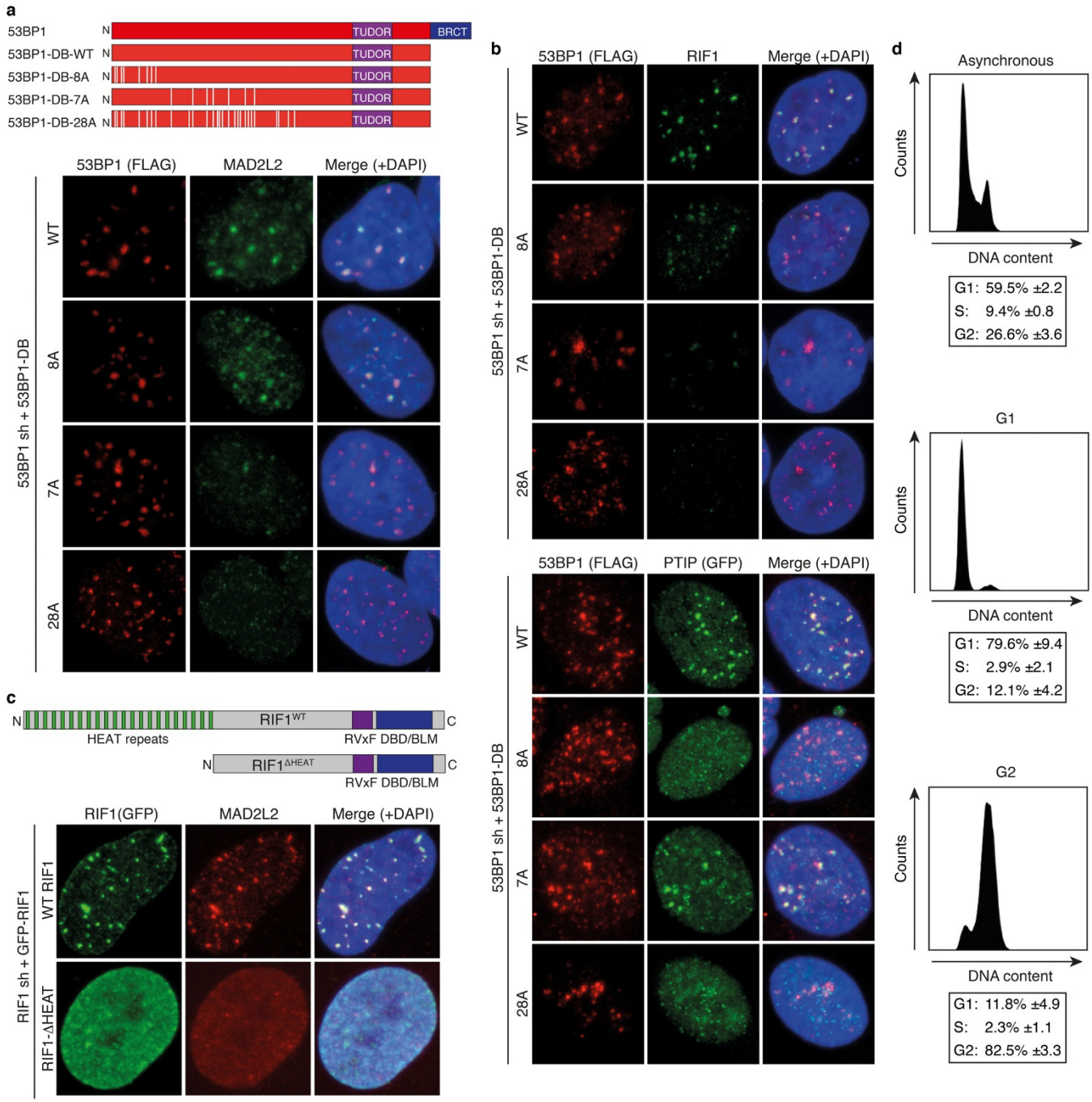

Extended Data Figure 9 | Related to Fig. 4. **a**, Schematic representation of the 53BP1 alleles with wild-type and substituted S/TQ sites used to address MAD2L2 IRIF localization dependence on 53BP1. Representative immunofluorescence images are displayed that show colocalization of endogenous MAD2L2 with 53BP1-DB-WT and -8A, but not with 53BP1-DB-7A or -28A. Quantifications are provided in Fig. 4f. **b**, Top, representative immunofluorescence images showing colocalization of endogenous RIF1 with 53BP1-DB-WT and -8A, but not 53BP1-DB-7A or -28A. Quantifications are presented in Fig. 4f. Bottom, representative immunofluorescence images showing colocalization of PTIP–GFP with 53BP1-DB-WT and -7A, but impaired colocalization of PTIP–GFP with 53BP1-DB-8A or -28A. **c**, Schematic representation of GFP-tagged wild-type RIF1 and GFP-tagged RIF1 lacking the N-terminal HEAT repeats (ΔHEAT), used to address MAD2L2 IRIF localization dependence on the HEAT repeats of RIF1. Representative immunofluorescence images are shown. Quantifications are presented in Fig. 4g. **d**, Cell cycle phase distributions of the RPE cells used in Fig. 4h to address cell cycle dependence of endogenous RIF1 and MAD2L2 localization to IRIFs ($n = 3$, mean ± s.d.). Original magnifications, ×63 with zoom factor 5.

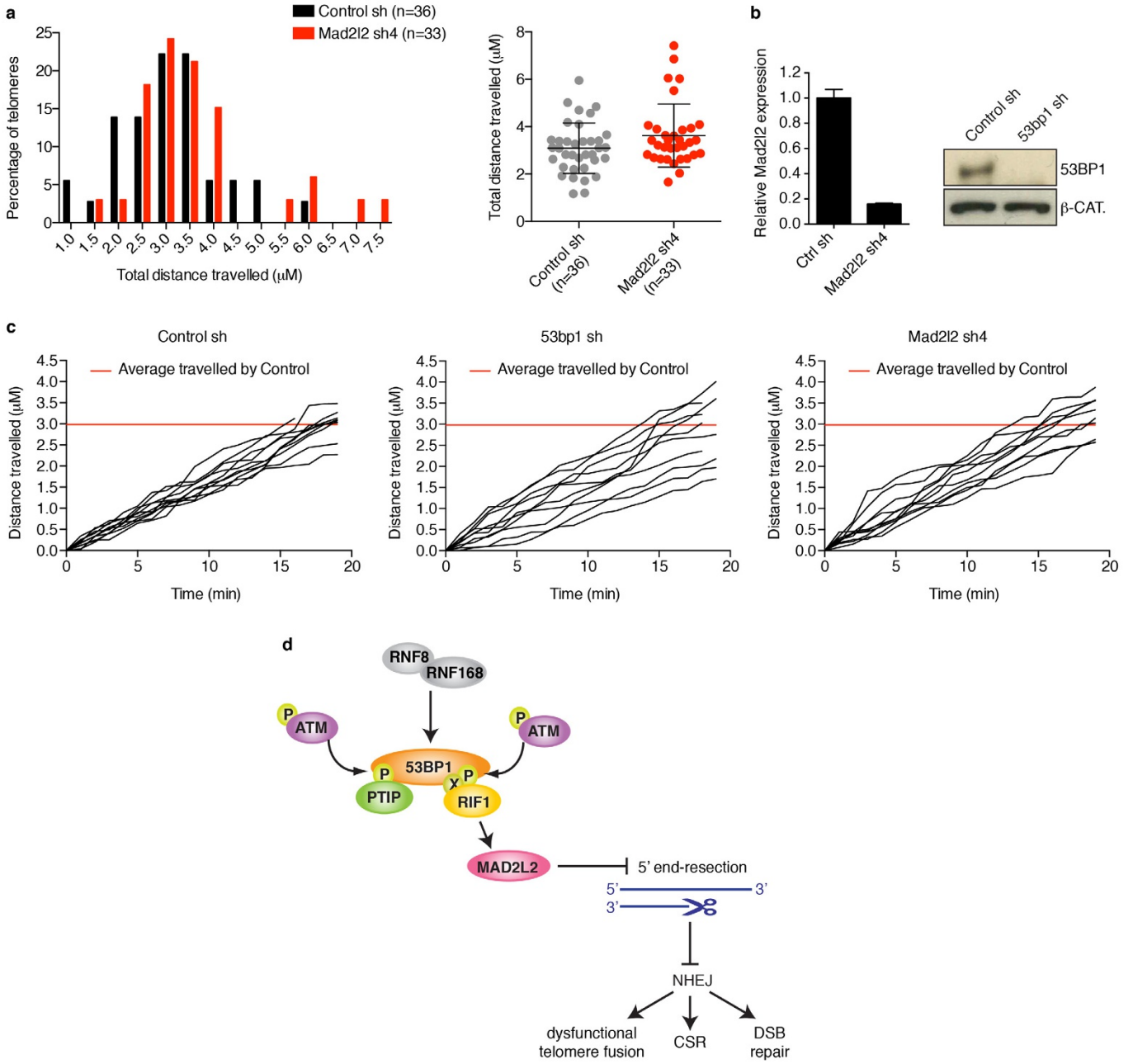

Extended Data Figure 10 | Related to Fig. 4. **a**, Frequency distribution (left) and scatter plot (right) of total distances travelled by uncapped telomeres in control or *Mad2l2* knockdown cells. **b**, qRT–PCR analysis of *Mad2l2* expression levels and western blot analysis of 53BP1 proteins levels in TRF2ts cells used in the experiments shown in **a** and **c** (error bars denote ± s.d.). **c**, Distance travelled by 10 representative uncapped telomeres for each condition. While multiple uncapped telomeres in 53BP1-depleted cells have reduced mobility, this is not seen for uncapped telomeres in MAD2L2-depleted cells. **d**, Model of the role of MAD2L2 in promoting NHEJ.